Author version: *Geol. Mag., vol.148(3); 2011; 404-422*

Geochemical investigation of gabbro from slow-spreading Northern Central Indian Ocean Ridge, Indian Ocean

DWIJESH RAY[1], SAUMITRA MISRA[2, *], RANADIP BANERJEE[3] & DOMINIQUE WEIS[4]

[1]National Centre for Antarctic and Ocean Research, Goa- 403804, India

[2]School of Geological Sciences, University of KwaZulu-Natal, Durban- 4000, South Africa

[3]National Institute of Oceanography, Goa-403004, India

[4]Pacific Centre for Isotope and Geochemical Research, University of British Columbia, Canada

Abstract

Gabbro samples (ca. < 0.4 Ma old) dredged from close to the "Vityaz Megamullion" on the slow spreading Northern Central Indian Ridge (NCIR, 18-22 mm/yr) include mostly olivine gabbro and Fe-Ti oxide gabbro. The cumulate olivine-gabbro shows ophitic to subophitic texture with early formed plagioclase crystals in mutual contact with each other, and narrow range of compositions of olivine (Fo_{80-81}), clinopyroxene (magnesium number: 85-87) and plagioclase (An_{67-70}). This olivine gabbro could be geochemically co-genetic with the evolved oxide-gabbro. These gabbro samples are geochemically distinct from the CIR gabbro occurring along the Vema, Argo and Marie Celeste transform faults and can further be discriminated from the associated NCIR basalts by their clinopyroxene (augite in gabbro, and diopsidic in basalts) and olivine (gabbro: Fo_{80-81}, basalts: Fo_{82-88}) compositions. Our major oxide, trace element and REE geochemistry suggest that the gabbro and the NCIR basalts are also not co-genetic and had experienced different trends of geochemical evolution. The clinopyroxenes of the present NCIR gabbros are geochemically similar to primitive melt that is in equilibrium with mantle peridotite, and do not show any poikilitic texture with resorbed plagioclase, which negate the possibility of these gabbros being a pre-existing cumulate that has been brought up to the shallower oceanic crust and interacted with the NCIR basalt. The Sr, Pb and Nd isotopic data of the gabbro substantially differ from those of the NCIR basalts and suggest significant contamination of its depleted mantle source most likely by the Indian Ocean pelagic sediments. The proportion of pelagic sediment that mixed in the depleted mantle source of the NCIR gabbro is much higher than the level of contamination observed for the Indian Ocean MORBs.

Keywords: Indian Ocean Ridge (IOR), IOR gabbro, IOR basalt, Depleted mantle, Pelagic sediment mixing.

1. Introduction

The study of the gabbroic rocks occurring along mid-ocean ridges is key for evaluating the evolution of the oceanic lithosphere as they record the succession of magmatic events from deep to shallow crustal levels. It is important that the magmatic processes that can influence the compositions of lavas erupted at the spreading centers, e.g. crystal fractionation, crystal accumulation, *in-situ* fractionation (Langmuir, 1989) and magma mixing, are likely to be recorded in the gabbroic rocks constituting the foundation of the oceanic crust. Dredged gabbroic samples, therefore, are studied to examine gabbro-basalt relationships (Tiezzi and Scott, 1980; Bloomer et al., 1989), conditions of crystallization (Elthon, 1987), compositions and diversity of parental melts (Bloomer et al., 1989) and the dynamics of crystallization of plutonic rocks (Bloomer et al., 1989; Meyer et al., 1989).

The recovery of gabbroic rocks is mostly restricted to major transform faults or fracture zones transecting mid-ocean ridges, e.g., Mid-Atlantic Ridge (Miyashiro and Shido, 1980; Teiezzi and Scott, 1980; Walker and Delong, 1984; Casey, 1997; Casey et al., 1998; Shipboard Scientific Party, 2004), Southwest Indian Ridge (Hebert et al., 1991; Dick et al., 1999, 2000), East Pacific Rise (Vanko and Batiza, 1980; Hebert et al., 1983; Früh-Green et al., 1996), Cayman Rise (Elthon et al., 1982; Elthon, 1987), Gakkel Ridge (Gao et al., 2003). Restricted exposures of gabbros in these tectonic setting are due to thinning of crust, poor magma supply or intense faulting. Gabbros reported from ultra-slow mid-oceanic ridge, e.g., the Gakkel Ridge in the Arctic Ocean, are mostly olivine gabbro, troctolite and microgabbro and are very primitive in nature (Gao et al., 2003). In contrast, gabbros from Mid-Atlantic and Southwest Indian Ridges (SWIR), occurring in association with major transform faults, are characterized by a wide range of composition that suggests closed-system fractionation in ephemeral melt intrusions emplaced in the axial lithosphere (Bloomer et al., 1989). The presently available whole-rock and trace-element data for oceanic gabbros are mostly restricted to certain areas (mostly in different ODP sites and oceanic core complexes) for evaluating these rocks.

The most well studied gabbro of Indian Ocean Ridge System (Fig 1) is ODP leg 118 from SWIR (Dick et al., 2002; Coogan et al, 2001). Gabbro from Leg 179 (ODP Hole 735B from Atlantis II fracture zone, Dick et al., 2000) and Leg 179 (Hole 1105A) near Leg 118 have also been studied extensively (Thy, 2003). Data from the above mentioned sites suggest that generation of oceanic crust through the SWIR took place by the continuous intrusion and reintrusion of numerous, small rapidly crystallized magma bodies together with complex interaction of magmatic, tectonic and hydrothermal processes (Dick et al., 1992). More recent studies on gabbroic rocks from Leg 179 (Hole 1105A) report the presence of both oxide-bearing and oxide-free olivine gabbro and gabbro (Casey et al., 2007). These gabbros of cumulate origin show well-layered structure and significant numbers of

mappable layer contacts or compositional contacts. The extent of fractionation represented by the gabbroic rocks and scare granophyres in the section is much greater than that represented in the Atlantis II basalt. The oxide phases are generally present in the more fractionated gabbroic rocks and absent in the more primitive gabbro members. Previously studied gabbroic rocks from the Central Indian Ridge have been recovered mostly from major transform faults (TF), e.g. Vema, Argo and Marie Celeste TF (Engel and Fisher, 1975; Bloomer et al., 1989). The heterogeneous textures and mineralogy and the distribution of gabbros in the Indian Ocean fracture zones indicate that many of them formed in small dykes or sills, rather than in large open magma chambers (Bloomer et al., 1989). Pulses of magma passing through such small dykes or sills may represent the ascent of a magma pulse of primitive nature from the mantle over a long period of time, or the ascent of several primitive magma batches separated in space and time (Bloomer et al., 1989).

The focus of the present paper is on the geochemistry of gabbros collected from the Northern Indian Ocean Ridge (NCIR) at 5°S-68°E (Fig. 1). The Chainbag dredging technique was used to collect these samples where the water column depth was ~3000 m. As the geochemistry of oceanic gabbro from NCIR is not adequately represented in the literature, their whole-rock analyses along with their petrographic and mineralogic descriptions are presented for the first time in this paper. One of the important objectives of this paper is to examine the possible petrogenetic relationship between the NCIR basalts (Ray et al., 2007) and these gabbros, which may be of three types: (a) These gabbros may be the pre-existing cumulate phase that are brought to the shallower level of oceanic crust and reacted with the NCIR basalt (cf. Lissenberg and Dick, 2008); (b) the present gabbro may be the cumulate phase derived during fractionation of the NCIR parent magma; or (c) these gabbros may have a different magmatic history and are genetically related to the gabbroic rocks occurring along transform faults.

Basalts generated at the Indian Ocean ridge have long been known to have isotopic compositions distinct from the Atlantic and Pacific MORBs (e.g. Subbarao and Hedge, 1973; Dupré and Allègre, 1983). The Indian Ocean basalts are characterized by relatively high $^{87}Sr/^{86}Sr$ (0.702733-0.703383) and low $^{206}Pb/^{204}Pb$ (17.898-18.839) (Mahoney et al., 1989), particularly for a given $^{143}Nd/^{144}Nd$, $^{207}Pb/^{204}Pb$ or $^{208}Pb/^{204}Pb$ value, compared to those of the Atlantic and Pacific MORBs (e.g. Price et al., 1986; Dosso et al., 1988; Mahoney et al., 1989). The origin of these isotopic signatures has long been a source of controversy, having been variously attributed to addition of plume material, deeply recycled pelagic sediments, subduction modified mantle wedge material and/or the addition of continental lithosphere to the Indian Ocean upper mantle (e.g., Mahoney et al., 1989;

Rehkamper and Hofmann, 1997; Kempton et al., 2002; Hanan et al., 2004). To explore these possibilities, we also measure the Pb, Sr and Nd isotope ratios of two NCIR gabbro samples to evaluate any possible input in the mantle reservoir (as in the Indian Ocean MORB, Rehkamper and Hoffman, 1997) during the gabbro genesis.

2. Regional geomorphology

The ocean bottom morphology of the present sampling area (Fig. 1) is described in detail in Drolia and DeMets (2005). The morphologic feature close to the inner northeastern corner of the Vityaz transform fault (Fig. 1b) includes an elongated domal high with well-expressed ridge-perpendicular corrugations. The megamullion rises from the ~4700 m deep rift axis to a depth of ~2300 m over a distance of 9 km with an inward-facing slope of 20^{o}. At distance beyond ~13 km from the ridge axis the slope reverses and the surface of the megamullion tilts gently (1.5^{o}) away from the spreading axis. Although Vityaz megamullion has been interpreted as an active detachment fault within the relatively poorly magmatic spreading segments at the NCIR (Drolia and DeMets, 2005), recent studies show that late stage volcanism, as found in the present case, plays an important role in the accretionary processes (cf. Morishita et al., 2009). The active detachment surface of the Vityaz megamullion facilitated extension and enhanced magma intrusion periodically within the relatively magma starved ridge segments (cf. Ildefonse et al., 2007). Such a possibility of gabbroic intrusion cannot be ruled out in present case as well.

The seafloor fabric in the study area is mostly dominated by abyssal hills and transform–parallel lineation, although some disturbed seafloor fabrics flanking the spreading segment immediately north of the Vityaz transform fault are also present (Drolia et al., 2003). The half spreading rate of the present location varies from 18 to 22 mm/yr (Drolia et al., 2003), typical for a slow-spreading crust. The perpendicular distance of the present study area from the nearest NCIR axis (Fig. 1b) is ~7.4 km. At the assumed half spreading rate (i.e. 18 mm/ yr), the oceanic crust in the present area has an estimated age of ~0.4 Ma. This perhaps indicates the maximum age limit of the gabbro body under study if it occurs as an intrusive dyke or sill (cf. Bloomer et al., 1989).

3. Sampling and Analytical Techniques

The present dredge location was situated at the northeastern corner of the 'Vityaz megamullion' adjacent to the non-transform discontinuity (Fig. 1b). The chain bag dredge technique was used to collect the rock samples, and the operation was carefully monitored by single beam as well as multibeam swath bathymetry during sampling. The chain-bag dredge was deployed about ~7.5

km away from the axial valley adjacent to the 'Vityaz Megamullion'. The precise navigational data on the time and position of the operation were recorded by onboard Global Positioning System.

In our chain bag dredge recovery, gabbro was the principal rock type (~80%). Other types included only altered basalts (~20%), which are not considered in the present study. In hand specimen study, the gabbro samples look very fresh, hard and compact. The major mineral phases of the gabbro (i.e., plagioclase, olivine and clinopyroxene), were analyzed using an electron microprobe with wave-length dispersive spectrometers (CAMECA SX 100) at the Central Petrological Laboratory, Geological Survey of India, Kolkata, India. The analytical conditions were: operating voltage 15 kV, sample current 12 nA, beam diameter 5 µm, and analysis duration for each element 10 sec. All calibrations were made using natural standards supplied by BRGM (Bureau de recherches géologiques et minières, France), except for Mn and Ti for which synthetic standards were used. The obtained data were corrected internally using the matrix correction procedure of Pouchou and Pichoir (1988) (PAP correction).

The samples for the whole-rock chemical analyses were ground to a 200 mesh size using tungsten carbide ring mill following the procedure of Balaram et al. (1999). The major element analyses of whole rock samples were carried out at the XRF laboratory, National Geophysical Research Institute, Hyderabad, India, using powdered homogeneous sample in pellet form. For XRF studies a Philips Magix XRF spectrometer PRO model PW2440 has been used in wavelength dispersive mode. The uncertainties of our analyses were better than±0.02 wt% on pressed powder pellets. The accuracy and precision of our XRF analyses as observed on the international rock standard the 'Mount Royal Gabbro, Canada' (MRG-1) were better than 5%, except for Mn and P for which the values are better than 8 % due to their low abundances. All trace elements including REE were analyzed from the same sample powders using ICP-MS (model ELAN DRC II, PerkinElmer Sciex Instruments, USA) at the National Geophysical Research Institute, Hyderabad, India, using methods described in Balaram et al. (1999). The accuracy and precision of measurements of these trace elements for international rock standard MRG-1 were better than ±5%.

The Sr, Pb, and Nd isotopic analyses were performed at the Pacific Centre for Isotope Research, Canada, using methods described by Weis et al (2005, 2006, and 2007). All the samples were carefully leached to remove all possible secondary alteration phases following the method described by Weis and Frey (1996) and by Nobre-Silva et al. (2009). The standard analyses during the course of this study gave: $^{87}Sr/^{86}Sr$= 0.710249 ± 14 (n=7) for NBS987 (TIMS Finnigan Triton); $^{143}Nd/^{144}Nd$= 0.511869 ± 18 for La Jolla Nd (MC-ICP-MS Nu Instruments), normalized to Rennes $^{143}Nd/^{144}Nd$ = 0.511973 (n=25), $^{206}Pb/^{204}Pb$= 16.9398 ± 24, $^{207}Pb/^{204}Pb$=15.4953 ± 19 and $^{207}Pb/^{204}Pb$=

36.7095 ± 46 (n=11) for SRM 981 (MC-ICP-MS Nu Instruments). For the MC-ICP-MS analyses, the measured results were normalized to the standard values on the basis of the mean of the day for Nd and by the ln-ln method for Pb, relative to the triple spike values of Galer and Abouchami (1998).

4. Petrography

The NCIR gabbros, in general, are coarse grained rocks exclusively composed of plagioclase, olivine, clinopyroxene, and Fe-Ti oxide (ilmenite and/or magnetite) in variable proportions. Depending on the modal proportions of the constituent minerals (Table 1), the gabbroic rocks can primarily be classified into two broad groups, viz.; (a) olivine gabbro, and (b) Fe-Ti oxide gabbro.

Most of the olivine gabbro shows typically ophitic to subophitic texture, with early formed plagioclase crystals are in mutual contact with each other and the late formed olivine and clinopyroxene grains occupy interstitial spaces (Fig. 2a). The plagioclase crystals also show triple junctions among three grain boundaries (Fig. 2b). This textural observation suggests cumulate origin of the gabbro (cf. Irvine, 1982; Winter, 2001). The interstitial clinopyroxenes sometimes contain partially digested subhedral prismatic plagioclase (Fig. 2c). Plagioclase, the most common mineral phase, occurs as subhedral tabular grains (0.7 to 6.3 mm in size) with well developed twin lamellae. Olivine (0.5 to 3.7 mm in size) is the next most dominant mineral and is intensively fractured with alteration stains (reddish brown in colour) sometimes present along inherent fractures. In places olivine contains partial or complete inclusions of plagioclase and clinopyroxene. The degree of alteration present along the fractures within the olivine varies between 5 and 10%. In comparison, plagioclase and clinopyroxene are almost alteration-free. Under microscope, all of our studied samples are fresh and show practically no sea water alteration.

The Fe-Ti oxide gabbro contains considerable proportions of Fe-Ti oxides in addition to plagioclase and clinopyroxene. The Fe-Ti oxides mostly occur as disseminated grains or sometimes as bands alternating with feldspar and clinopyroxene-rich layers (Fig. 2d). A third and rare variety is microgabbro or fine-grained gabbro, which is principally composed of equigranular plagioclase and less abundant clinopyroxene grains. In addition to fine grain size, the microgabbro differs from the olivine gabbro by conspicuous absence of olivine.

Lissenberg and Dick (2008) recently pointed out a possibility that some oceanic gabbros might be pre-existing gabbros that have reacted with migrating melts. This type of gabbro typically shows poikilitic texture with abundant high Mg# (86-91) clinopyroxene, which occurs as oikocryst enclosing olivine and resorbed plagioclase. In this type of melt-rock interaction, gabbro xenoliths contain quenched glass pockets (Gurenko and Sobolev, 2006). In the Bay of Islands ophiolite, extensive

disaggregation and mixing between gabbros and invading magmas was noticed that produced a range of hybrid rocks (Bédard, 1991; Bédard and Hebert, 1996; Bédard et al., 2000). Our gabbro samples, however, are dominated by ophitic to subophitic texture (Fig. 2a), and no poikilitic clinopyroxene is seen under microscope. Neither any evidence of quenched glass pocket nor any petrological evidence of mixing between our gabbro and invading melt is observed in our sample population. So the hand specimen and textural evidence do not suggest a pre-existing cumulate origin of our gabbro samples. Gabbro xenoliths in MORB from the East Pacific Rise show textural features of extensive melt-rock interaction, and it has been suggested that this interaction plays an active role underneath the East Pacific Rise (Ridley et al., 2006). Our collected samples of NCIR basalts, however, do not show any xenolithic gabbro in hand specimen or any petrographic evidence of melt-rock interaction (Ray et al., 2007). Therefore, it can be concluded that melt-rock interaction is perhaps not important in the evolution of the NCIR MORBs.

5. Analytical data

5.a. Mineral chemistry

Selected microprobe analyses of different mineral phases of the NCIR olivine gabbro are given in Table 2 (and appendix) along with analyses from NCIR basalts for comparison. The unzoned olivines of the olivine-gabbro show uniformity in composition with ~Fo_{80-81} compared to the olivine phenocrysts of NCIR basalt (Fo_{81-88}). There are no notable variations between the core and rim of olivine (core~Fo_{80} and rim~Fo_{78}). The plagioclase in olivine gabbro shows restricted compositional variation between An_{67} and An_{75} which overlaps with the lower range of composition of plagioclase phenocrysts in the NCIR basalts (An_{63} to An_{88}). The clinopyroxenes of the olivine gabbros have composition of $Wo_{40-45}En_{48-52}Fs_{8-9}$ and plot in the augite field of pyroxene quadrilateral, with a limited linear Ca-enrichment trend that is sub-parallel to the En-Di join (Fig. 3). On the other hand, the clinopyroxenes of the NCIR basalts have an average composition of $Wo_{49}En_{32}Fs_{19}$ and show a limited Fe-enrichment trend parallel to the Di-Hd join within the diopside field. The Mg# [100* mole Mg/ (mole Mg+ mole Fe)] of the clinopyroxene from gabbro exhibits a restricted variation between 87 and 85, while those from the NCIR basalts show a wide variation from 73 to 51 (Table 2).

The olivines in Fe-Ti oxide gabbro (Fo_{78-80}) are marginally Fo-poor in average in comparison to those of olivine-gabbro (Fo_{80-81}) and NCIR basalt (Fo_{81-88}) (Table 2). The plagioclase and clinopyroxene of the Fe-Ti oxide gabbro overlap in composition to those of olivine-gabbro (Figs 3a, b). The plagioclase of the Fe-Ti oxide gabbro contains marginally higher FeO_{total} (~0.13 wt% in average) compared to those of the olivine gabbro and is comparable to those of the CIR gabbro of Bloomer et al. (1989) (Table 2, Fig. 4a). One of the plagioclase analyses (Table A2 in appendix,

sample number Gabbro-3f) show presence of relatively high FeO_t (0.77 wt%), which could be due to relatively high proportion of replacement of Al by Fe^{3+} ion in the plagioclase structure (cf. Deer, Howie and Zussman, 1992). The clinopyroxenes of the Fe-Ti oxide gabbro, CIR gabbro of Bloomer et al. (1989) and olivine-gabbro together show linear and curvilinear decreasing trends of variations in Mg# versus Al a.p.f.u. (atoms power formula unit) and Cr respectively where clinopyroxenes from the Fe-Ti gabbro and olivine-gabbro always represent the most and the least evolved member respectively along these trends (Fig. 4b, c).

The compositions of pyroxenes of the NCIR gabbros and basalts are compared with the experimental pyroxene compositions of Villiger et al. (2004) obtained during fractional and equilibrium crystallization of primitive, mantle-derived tholeiitic basalt at 1.0 GPa (Fig. 3). A comparison of our samples with the above experimental work (Villiger et al., 2004) is reasonable because the primitive NCIR parent basaltic magma is found to have evolved at a pressure of ~1 GPa (Ray et al., 2007). Our least evolved clinopyroxene of the NCIR gabbro lies close in composition to the clinopyroxenes of Villiger et al. (2004), and our clinopyroxenes are found to have evolved between temperatures of 1200 and 900^oC when compared with the isotherms on pyroxene quadrilateral after Lindsley (1983). The trend of clinopyroxenes of the NCIR basalt, on the other hand, is parallel to the trend of clinopyroxene of Villiger et al. (2004) obtained during their fractional crystallization experiment, although these pyroxenes are systematically Ca-enriched. The clinopyorxenes of NCIR basalt evolve at relatively low temperature at $\leq 800^oC$.

Our additional evidence against origin of the clinopyroxenes of the olivine and oxide gabbros by melt-rock interaction (cf. Lissenberg and Dick, 2008) is shown in the TiO_2 versus Cr_2O_3 plot (Fig. 4d). In this diagram, the clinopyroxenes of the olivine and oxide gabbros occur in the field of the primitive melts that is in equilibrium with mantle peridotite. The clinopyroxenes of the olivine- and oxide gabbros have nearly the same TiO_2 contents (~0.35 wt%), but the former has much higher Cr_2O_3 (~ 1 wt% in average) compared to the latter (~0.19 wt%). The clinopyroxenes of olivine gabbro define a linear trend, on which the clinopyroxenes of oxide gabbros are plotted. This plot therefore suggests co-genetic relationship of clinopyroxene of olivine and oxide gabbros and crystallization of these clinopyroxenes from mantle-derived primary magma rather their formation by any melt-rock interaction as suggested by Lissenberg and Dick (2008).

5.b. Whole rock chemistry

5.b.1. Major element chemistry

The major and trace element compositions along with Sr, Pb and Nd isotopic ratios of the

present NCIR gabbro are shown in Table 3. The Mg# of the olivine gabbro samples vary over a range of ~85 to 78, while the Fe-Ti oxide samples have lower values of 68 and 51 (Fig. 6). In comparison, the early reported CIR gabbros, collected from Vema, Argo and Marie Celeste TF and ANTP 125-8 sites, have comparable compositions except for one sample with very low Mg# (~39) (Engel and Fisher, 1975).

The possible liquid line of descent between the present gabbro (cumulates) and NCIR basalt is also examined in the normative olivine-diopside-silica diagram projected from the plagioclase apex (after Walker et al., 1979) (Fig. 5). The evolved NCIR basalts, having Mg# < 0.68, plot on a linear trend, which is parallel to the 1 GPa cotectic line between Di and Ol fields but within the Di field. The olivine gabbro samples show a point concentration of data on the Ol-Di cotectic line at 1 GPa, but two samples of oxide gabbro show wide scatter in plot. Neither the gabbro nor the NCIR basalts (Mg# < 0.68) describe any liquid line of descent in this diagram indicating their non-cogenetic origin.

The major oxide variations between NCIR gabbros and basalts are also examined in Mg# versus major oxide bivariant plots (Fig. 6). The variations of SiO_2 for both the olivine- and Fe-Ti oxide gabbros as well as the NCIR basalts are very restricted between ~46 and 50 wt% and are independent on any variation of Mg# (Fig. 6a). In the major element binary plots against Mg#, significant and systematic variations are observed only for Al_2O_3 and CaO. Distinctly different but parallel decreasing trends are observed for Al_2O_3 and CaO with decreasing Mg# for the present gabbro and the CIR gabbro (Engel and Fisher, 1975) where the CIR gabbro always have higher oxide values with reference to the same Mg# (Figs. 6b,c). In the Mg# versus CaO plot, the trend of the gabbro is linear, although some scatter of data is also seen, which is possibly related to the variation in An content in plagioclase in our studied samples. The NCIR basalts along with its primitive members show a distinct cluster in the Mg# versus Al_2O_3 plot, right above the linear trends defined by these two sets of gabbro samples. In the Mg# versus CaO plot, the average linear trend defined by the NCIR basalt is parallel to those of the present and CIR gabbros and lying in between them. In the Mg# versus Na_2O and P_2O_5 plots, the gabbroid rocks define moderately increasing linear trends with decreasing Mg# (Figs. 6d, e). The CIR gabbro (Engel and Fisher, 1975), for comparison, defines different trends in both these diagrams. Most of the CIR gabbro has relatively high Na_2O and low P_2O_5 compared to the present gabbro with reference to the same Mg#. The NCIR basalts have a tendency to cluster above the present gabbro trends. The available primitive NCIR N-MORB (Mg#>0.68, Ray et al., 2007) also forms clusters in these diagrams that are not overlapping with the fields of the NCIR basalt. In MgO versus TiO_2 plot, the NCIR basalts and most of the present gabbro samples (except gabbro-3 in Table 3) show linear increasing trends of varying slope with decreasing MgO (Fig. 6f). Different

linear trends in the entire major oxide variation diagrams for the limited numbers of present gabbro and the CIR gabbro (Engel and Fisher, 1975) (Fig. 6) primarily suggest that these two plutonic igneous rocks have different liquid line of descents. The NCIR basalts also do not show any genetic relation with either of the gabbroic rocks (Fig. 5, 6).

5.b.2. Trace element chemistry

The CI-chondrite normalized (after McDonough and Sun, 1995) incompatible trace element chemistry of the NCIR gabbro and basalt is compared in a spidergram (Fig. 7). The olivine gabbros are mostly depleted in REE (La, Ce, Yb, Lu) and HFS elements (Nb, Nd, Zr, Hf) compared to the average NCIR N-MORB. The oxide gabbros, on the other hand, are less depleted and more MORB-like. Some of the LIL elements (Rb, K) in the gabbros have comparable abundances to that of the average NCIR MORB. Additionally, all the gabbros are uniformly enriched in Ba (~5 to 6 times NCIR MORB) and have variable Nb (~0.02 to 3 times NCIR MORB). The absence of any complementary incompatible element geochemistry between the NCIR gabbro and the average NCIR N-MORB in general, therefore, does not favour any model of crystal fractionation for the generation of these two igneous rocks from common parent magma.

Any possible geochemical trends described by our limited number of gabbro samples (n=6) are compared with those of NCIR basalts in Mg# versus incompatible and compatible trace element plots (Fig. 8). In all of our plots, the trends and variations defined by the gabbro samples are mostly described by the oxide gabbro (n=2). In the Mg# versus Zr plot, the gabbros (Zr ~ < 85 ppm) show linearly increasing trend with decreasing Mg#, the NCIR basalts have relatively high Zr (~60-150 ppm) and show, in general, a relatively steep increasing linear trend with decreasing Mg# although minor variations exist (Fig. 8a). The NCIR basalts with Zr contents of ~80 and 140 ppm show additional horizontal trends with no variation of Zr with increasing Mg#. In the Mg# versus Y plot, although the NCIR basalts show cluster on the linear trend defined by the present gabbro, they define two different linear trends with no change of Y content (at ~30 and 42 ppm Y) with increasing Mg# (Fig. 8b). In Mg# versus Cr and Ni plots, Cr and Ni show decreasing curvilinear and linear trends respectively for the gabbros with decreasing Mg# (Fig. 8c, d). In these plots, the NCIR basalts show evolved chemistry comparable to the Fe-Ti oxide gabbro. Though the basalts form clusters on the trends defined by the gabbro samples, they show no variations in Cr and Ni contents with decreasing Mg#.

In the CI-chondrite-normalized (after McDonough and Sun, 1995) REE spidergram, the olivine- and Fe-Ti oxide gabbros show slightly middle REE up convex pattern (La/Yb= 0.42-0.9) with

the latter having distinctly higher total REE (Fig. 9a). In general, the olivine gabbros are marginally LREE depleted (La/Sm_N= 0.33-0.62) with almost flat HREE (Gd/Yb_N=1.26-1.55) and show a positive Eu anomaly {Eu/Eu*= 1.13-2.06, calculated after Taylor and McLennan (1985) using following formula: $Eu_{anomaly}= (Eu_{CN})/[(Sm_{CN})*(Gd_{CN})]^{0.5}$}, which is almost absent in the oxide gabbro. The Fe-Ti oxide gabbro also has marginally depleted LREE (La/Sm_N= 0.33-0.50) and flat HREE (Gd/Yb_N= 1.27-1.37) but without any Eu anomaly. In contrast, the average NCIR N-MORB has flat REE (La/Yb_N=0.91). In total REE (La, Ce, Nd, Sm, Eu, Gd, Dy, Er, Yb and Lu ~ΣREE) content, the olivine gabbros have the lowest values (< 8.5 ppm) and the oxide gabbros have higher values (22 and 48 ppm) that overlap with those of the NCIR N-MORB (Fig. 8b). In the Mg# versus total REE plot, the NCIR gabbro and basalt, however, show distinctly different increasing linear trends for total REE with decreasing Mg# (Fig. 9b).

The incompatible versus compatible trace element variation diagrams are often used to examine the magmatic process (Cocherie, 1986). Though originally proposed for volcanic rocks (Treuil and Varet, 1973; Allègre et al., 1977; Villemant et al., 1981), Cocherie (1986) systematically studied the behaviour of trace elements during evolution of plutonic rock suites to evaluate fractional crystallization, partial melting and magma mixing. It is already understood that the NCIR basalts were formed by fractionation of one of the primitive MORB (no. 525-5-3) of Presnall and Hoover (1987) (Ray et al., 2007). The compatible versus incompatible trace element diagrams (after Cocherie, 1986) have, therefore, been used in the present study to evaluate the liquid line of descent of the NCIR basalts and its relationship with the present NCIR gabbro (Fig. 10). The governing criterion for selection of elements for our plots is very high ranges of variation of the elements in both gabbros and basalts. In the log-log plots of Ni and Cr against Zr, both the NCIR gabbro and basalt show similar but different decreasing linear trends for Ni and Cr with increasing Zr (Fig. 10a, b) indicating non-cogenetic origin of these rocks.

The covariation between the incompatible trace element ratios and the least compatible element between the two (after White, 1999) has also been examined between the NCIR basalt and gabbro for further verification of the possible co-magmatic nature of these two rock groups (Fig. 10c). In the Zr/Y versus Zr plot, the Zr/Y ratios of gabbro and basalt are different; the gabbros have a Zr/Y ratio mostly between ~1 and 2, and most of the data show a cluster at Zr ≤25 ppm; while the basalt has a characteristic value close to 3-4 and the values do not show much variation with increasing Zr. Different Zr/Y ratios of the present gabbro and basalt also favour their non co-genetic relation.

In summary, the present available petrological and geochemical data can be used to conclude the possible petrological relationships between our present olivine and oxide gabbro samples, and

between present gabbros and NCIR basalts. There are reasons to believe that the olivine- and oxide gabbros could be co-genetic because: (a) olivine, plagioclase and clinopyroxene in these two gabbro types either have similar bulk compositions or show systematic variation in bulk composition (Table 2, appendix, Fig. 3, 4), and (b) in major and trace element plots these two types of gabbro always show collinear trends (Fig. 6, 8, 9b, 10a, b).

The current geochemical data on the present olivine- and oxide gabbros (Table 2, 3 and appendix) and their logical interpretation listed below negate all possibility of the NCIR gabbro representing the cumulate phase resulting from fractionation of the NCIR parent magma: (a) the clinopyroxenes of the NCIR gabbro and basalt have completely different trends of evolution in pyroxene quadrilateral indicating their generation at widely different temperatures between 1200 and 1000^{o}C and at < 800^{o}C respectively (Fig. 3) and the olivines of the NCIR gabbro are less Mg-rich compared to those of the NCIR basalts (Table 2), which are not expected if these two rocks were co-genetic; (b) In the MgO (compatible) versus TiO_2 (incompatible) oxide plot, the primitive NCIR basalts, which are compositionally similar to one of the primitive basaltic member (No 525-5-3) of Presnall and Hoover (1987) (Ray et al., 2007), and the evolved NCIR basalts together constitute a liquid line of descent that is different in style from that of the present gabbro suite (Fig. 6f); (c) in the CIPW normative Di-Ol-Qtz plot (Fig. 5) and in the most of the major oxide bivariant diagrams against Mg#, the NCIR gabbro and basalt do not show any common geochemical lineage (Fig. 6a, b, c, d); (d) absence of any complimentary incompatible element geochemistry between the present NCIR gabbro and basalt (Fig. 7), (e) different trends of evolution of the NCIR gabbro and basalt are seen in Mg# versus Zr, Y, Cr, Ni and total REE plots (Fig. 8, 9b); (f) in compatible versus incompatible trace element plots (Fig. 10a, b) and in plot of incompatible trace elements ratio versus the least incompatible element of the two (Fig. 10c), the NCIR gabbro and basalt never show any common geochemical lineage. Therefore, on the basis of geochemical data, it can be argued that the NCIR gabbro represents a cumulate phase that was derived during fractionation of an unknown parent magma that was compositionally different from that of the NCIR basalt. The isotopic data in favour of this conclusion are discussed below.

6. Isotope Geochemistry

The isotopic signatures has long been used to explore any possible input in the mantle reservoir during generation of the NCIR parent magmas, which may be attributed to addition of plume material, deeply recycled pelagic sediments, subduction modified mantle wedge material and/or the addition of continental lithosphere to the Indian Ocean upper mantle (e.g., Mahoney et al., 1989; Rehkamper and Hofmann, 1997; Kempton et al., 2002; Hanan et al., 2004). Our present isotopic data on two olivine

gabbro samples have been used to explore these possibilities. As the present location (Fig. 1) is far from any known hotspot, we can perhaps negate the possibility of addition of any plume material in mantle reservoir to regulate NCIR mantle chemistry (also see Michard et al., 1986), although this type of interaction is only identified at the westernmost SWIR and near the Bouvet triple Junction (Kurz et al., 1998, 2009; Meyzen et al., 2007).

Hart et al. (1999), in their work on oceanic gabbro samples from site 735; situated on a shallow (700 m) wave-cut platform on the transverse ridge system east of Atlantis II fracture zone, SE Indian ridge; had identified sea water components in these samples in isotopic scales ($^{87}Sr/^{86}Sr$, $^{206}Pb/^{204}Pb$, $\delta^{18}O$, $^{187}Os/^{188}Os$). Their samples, which were occurring on ~11 to 12 Ma old oceanic crust, show petrological evidences of alterations up to amphibolite to greenschist facies. In contrast, our samples are very young in age (ca. < 0.4 Ma) and are almost alteration free (Fig. 2). The samples were also carefully leached to remove any possible alteration before isotopic analyses. Therefore, it is likely that the effect of sea water alteration on our gabbroic samples is minor and the present isotopic data (Table 3) can be used to evaluate their magmatic evolution. As our gabbro samples are very young in age (ca. < 0.4 Ma), we only consider the measured isotopic data of these samples in the following discussion.

Two olivine gabbro samples from the present suite show $^{87}Sr/^{86}Sr$ (0.702878-0.702919) and $^{143}Nd/^{144}Nd$ (0.513116-0.513119) ratios (Table 3) that are comparable to the average values of the SWIR gabbro (0.702921 and 0.51312 respectively; Hart et al. 1999). In contrast, Pb isotopic ratios, e.g. $^{206}Pb/^{204}Pb$ (18.4611-18.5316), $^{207}Pb/^{204}Pb$ (15.5392-15.5538) and $^{208}Pb/^{204}Pb$ (38.3850-38.4593), of present gabbro samples are relatively high as compared to the SWIR gabbro (17.662, 15.447 and 37.381 respectively) and the NCIR basalts (18.067, 15.456 and 37.870 respectively) (Table 3). Therefore, these isotopic data suggest that the NCIR and SWIR gabbros, and the NCIR basalts seem to have different mantle sources. The possibilities of contamination of ancient Indian Ocean Ridge (IOR) mantle with radiogenic pelagic sediments (Rehkamper and Hofmann, 1997) or by lower crustal component (Nakamura et al., 2006) have been discussed. In the present study, we explore this possibility for the NCIR gabbro mostly using the measured radiogenic isotopic ratios (Fig. 11).

The Nb/U and Ce/Pb ratios though considered sensitive indicators to evaluate crustal contamination of the mantle source in MORB glasses (Rehkamper and Hofmann, 1997), are likely to be insensitive so far as the IOR gabbroic rocks are concerned because these rocks represent cumulate phases and, therefore, the ratios are possibly influenced by magmatic processes. In the REE diagram, the NCIR gabbros plot between the most depleted D-mantle and the most enriched Indian Ocean pelagic sediments end members (Fig. 9a) and, therefore, mixing of these two end member components may probably have important bearing in the genesis of the NCIR gabbro. The incompatible La/Ce

ratio has been well used to evaluate magma mixing for the Reykjanes Ridge basalts (Langmuir et al., 1978). In our present study when the D-mantle (data from Hart, 1984), NCIR gabbro (Table 3), NCIR basalts (Rehkamper and Hofmann, 1997), and the Indian Ocean pelagic sediments (Ben Othman et al., 1989) are plotted together in the La/Ce_N versus $^{206}Pb/^{204}Pb$ diagram, they describe a well defined curvilinear mixing trend between D-mantle and pelagic sediment end members (Fig 11a) (cf. Langmuir et al., 1978). On this diagram, the NCIR basalt from literature (Rehkamper and Hofmann, 1997) always plot close to the D-mantle end member, whereas the two gabbro samples are plotted midway between the D-mantle and pelagic sediment. In the measured $^{206}Pb/^{204}Pb$ versus $^{208}Pb/^{204}Pb$ and $^{207}Pb/^{204}Pb$ plots, the olivine gabbro falls on a straight mixing line containing the depleted mantle (D) and the Indian Ocean pelagic sediment as end member compositions (Fig. 11b, c). These mixing lines are different from the Northern Hemisphere Reference Lines (NHRL) (Hart, 1984) with $\Delta^{207}Pb/^{204}Pb$ and $\Delta^{208}Pb/^{204}Pb$ values of our two gabbro samples of ~4.67, 5.40 and 43.49, 42.76 respectively. In Nd-Pb and Sr-Pb isotopic diagrams, the gabbro compositions also fall on a curvilinear hyperbolic trend between D-mantle and pelagic sediments (Figs. 11d, e).

The isotopic compositions of the present gabbros occurring within the active NCIR are indicative of their source rock composition. All the diagrams, therefore, suggest that the NCIR magmas were generated from a depleted mantle source that was contaminated by mixing of Indian Ocean pelagic sediments in moderate to high proportions. The proportion of pelagic sediments can be computed close to 9 wt% or less for the NCIR basalts (we used Pb isotope compositions of average D-mantle and Indian Ocean pelagic sediment for our computation, for calculation procedure see Faure and Mensing, 2005, p. 347), which is very close to the estimation of Rehkamper and Hofmann (1997) of ~10 wt%. For our two gabbro samples the proportion of involvement of the pelagic sediments, however, is much higher (could be ~50 wt%) as suggested by our Pb-isotope data.

7. Discussion

Occurrences of gabbros adjacent to the Vityaz megamullion of NCIR (i.e. low angle detachment fault, cf. Drolia and DeMets, 2005) represents recent magmatic intrusion. This intrusion creates the plutonic complex (the gabbro body apparently after a magmatically quiescent period, which is common in megamullion settings elsewhere (cf. Ildefonse et al., 2007). The presence of low angle detachment faulting facilitates the emplacement of the gabbro in this tectonic setting (cf. Dick et al., 2008). The dredged gabbro from the megamullion thus genetically differ from other CIR gabbros whose emplacement is exclusively controlled by the major transform faults, viz. Marie Celeste, Argo and Vema transform faults (Bloomer et al., 1989). The gabbros are mostly homogeneous in

compositions and vary between olivine gabbro and Fe-Ti oxide gabbros, in comparison to the other fracture zone gabbros of the Indian Ocean Ridge system, which have heterogeneous mineralogy and texture (Bloomer et al., 1989). The Vityaz gabbros also show different trends of evolution in Mg# versus major oxides plots (Fig. 6) compared to the CIR gabbros from the transform faults (Engel and Fisher, 1975). It appears that these two suites of gabbro samples have different petrogenetic evolutions. On the other hand, mineral chemistry (Table 2, Appendix, Fig. 3, 4) of olivine- and Fe-Ti oxide gabbros of the present gabbro suite, along with their geochemical continuity (Fig. 6, 8, 9) suggest that these two rock types could be co-genetic.

Any possibility of the present gabbro of being a pre-existing cumulate phase that is brought up to the shallower level of oceanic crust and reacted by the NCIR basalt can be ruled out due to (a) absence of poikilitic clinopyroxene, with resorbed plagioclase inclusions (Fig. 2c); and (b) the clinopyorxene composition of these gabbros is well within the field of primitive melt that is in equilibrium with mantle peridorite (Fig. 4d) (cf. Lissenberg and Dick, 2008).

Based on the Pb, Nb and Sr isotopic ratios, Rehkamper and Hofmann (1997) suggested that the parent magma of the Indian Ocean MORB was generated from a depleted mantle (mostly Atlantic or Pacific type) that had been contaminated by recycled ocean crust with ~1.5 Ga old pelagic sediments. In their model, the pelagic sediment input may vary up to ~10 wt%. Our present Pb, Sr, Nd isotopic ratios together with geochemical studies suggests the proportion of the pelagic sediment mixing might be ~9 wt% (Fig. 11). The mixing of the Indian Ocean pelagic sediments in the parent magma of the present gabbro suite is found to be significant, which is much higher compared to that of the Indian Ocean MORB source. However, the mechanism by which this high proportion of pelagic sediments was incorporated into the D-mantle during the genesis of the gabbro can not be clearly established.

8. Conclusion

1. The gabbro samples (ca. < 0.4 Ma) dredged from the slow spreading segment of the NCIR adjacent to the 'Vityaz megamullion' are mainly of two types: olivine and Fe-Ti oxide gabbros. Their common mineralogical compositions, i.e. olivine (~Fo_{80-81}), clinopyroxene ($En_{48}Fs_{8-10}$) and plagioclase (An_{67-70}); and geochemical continuity on major oxide and trace element variation diagrams suggest these two varieties of gabbros could be co-genetic.
2. The geochemical and Pb-isotopic data suggest that the present gabbro samples are not co-genetic with the NCIR basalts, and are also geochemically distinct from the CIR gabbro from the Vema, Argo and Marie Celeste transform faults.
3. Modeling on isotopic data suggests that the NCIR gabbros were derived from a depleted

mantle source that was significantly contaminated most likely by Indian Ocean pelagic sediments. The level of pelagic sediment contamination is much higher compared to that of the Indian Ocean MORB source.

Acknowledgements

We are grateful to D. Pyle, T. Morishita, H. Kumagai and P. Leat for their valuable comments on the early versions of the manuscript. We are obliged to Directors NCAOR and NIO for constant encouragements. We are indebted to Ministry of Earth Sciences, Government of India, for allotting the cruises and the scientific party and the crew members of ORV Sagar Kanya for their unstinted help in collecting the samples. This work is supported by the CSIR Network program and Office of Naval Research, USA. The first author (D. R.) also gratefully acknowledges the support of CSIR-Senior Research Fellowship during the progress of this research. A. K. Chakrabarti helped us on several technical aspects of this manuscript.

References

ALLÈGRE, C.J., TREUIL, M., MINSTER, J.F., MINSTER, B. & ALBAREDE, F. 1977. Systematic use of trace elements in igneous processes. Part I: Fractional crystallization processes in volcanic suites. *Contributions to Mineralogy and Petrology* **62**, 57-75.

BALARAM V., GNANESHWARA RAO, T. & ANJAIAH K.V. 1999. International proficiency tests for analytical geochemistry laboratories: an assessment of accuracy and precision in routine geochemical analysis. *Journal Geological Society of India* **53**, 417–423.

BEN OTHMAN D., WHITE, W.M. & PATCHETT, J. 1989. The geochemistry of marine sediments, island arc magma genesis, and crust-mantle recycling. *Earth and Planetary Science Letters* **94**, 1-21.

BÉDARD, J.H. 1991. Cumulate recycling and crustal evolution in the Bay of Islands ophiolite. *Journal of Geology* **99**, 225-249.

BÉDARD, J.H. & HEBERT, R. 1996. The lower crust of the Bay of Islands ophiolite, Canada: petrology, mineralogy and the importance of syntexis in magmatic differentiation in ophiolites and at ocean ridges. *Journal of Geophysical Research* **101**, 25105-25124.

BÉDARD, J.H., HEBERT, R., BERCLAZ, A. & BARFALVY, V. 2000. Syntexis and the genesis of the lower oceanic crust. In *Ophiolites and Oceanic crust: New insights from field studies and the Ocean Drilling Program*, Special Paper, **349**, (eds Dilek, Y., E.M. Moores, D. Eltohn & A. Nicolas), pp. 105-119. Geological society of America

BLOOMER, S.H., NATLAND, J.H. & FISHER, R.L. 1989. Mineral relationships in gabbroic rocks from fracture zones of Indian Ocean ridges: evidence for extensive fractionation, parental diversity and boundary layer recrystallisation. In *Magmatism in the ocean basins* (eds Saunders, A.D. and M.J. Norry), pp. 107-124. Geological Society of London, Special publication no. 42.

CARLO DE E.H. 1993. Geochemistry of pore water and sediments recovered from Leg 136, Hawaiian Arch. In *Proceedings of Ocean Drilling Program, Scientific Results* **136**, (eds Wilkens, R.H., J. Firth, J. Bender et al.), pp. 77-83. Ocean Drilling Program, College Station, TX.

CASEY, J.F. 1997. Comparison of major- and trace-element geochemistry of abyssal peridotites and mafic plutonic rocks with basalts from the MARK region of the Mid-Atlantic Ridge. In *Proceedings of Ocean Drilling Program, Scientific Results* **153** (eds Karson, J.A., M. Cannat, D.J. Miller and D. Elthon D), pp.181–241. Ocean Drilling Program, College Station, TX.

CASEY, J.F., BRAUN, M.G., FUJIWARA, T., MATSUMOTO, T., KELEMEN, P.B. & the Scientific Party 1998. Megamullions along the Mid-Atlantic Ridge between 14 and 16ºN: Results of Leg 1, JAMSTEC/WHOI Mode 98 survey, Eos Trans. AGU, 79, Fall Meet. Suppl., F920.

CASEY, J.F., BANERJI, D. & ZARIAN, P. 2007. Leg 179 synthesis: geochemistry, stratigraphy, and structure of gabbroic rocks drilled in ODP Hole 1105A, Southwest Indian Ridge. In *Proceedings of Ocean Drilling Program, Scientific Results* **179** (eds Casey, J.F. and D.J. Miller), pp.1–125, Ocean Drilling Program, College Station, TX.

COCHERIE, A. 1986. Systematic use of trace element distribution patterns in log–log diagrams for plutonic suites. *Geochimica Cosmochimica Acta* **50**, 2517–2522.

COOGAN L.A., MACLEOD, C.J., DICK, H.J.B., EDWARDS, S.J., KVASSNES, A., NATLAND, J.H., ROBINSON, P.T., THOMPSON, G. & O'HARA M.J. 2001. Whole-rock geochemistry of gabbros from the southwest Indian ridge: constraints on geochemical fractionations between the upper and lower oceanic crust and magma chamber processes at (very) slow spreading ridges. *Chemical Geology* **178**, 1-22.

DEER, W.A., HOWIE, R.A. & ZUSSMAN, J. 1992. An Introduction to the Rock-Forming Minerals, Longman Scientific and Technical, UK, 696pp.

DICK, H.J.B., ROBINSON, P.T. & MEYER, P.S. 1992. The plutonic foundation of a slow-spreading ridge, In *The Indian Ocean: A synthesis of results from the Ocean Drilling Program* Geophysical Monograph, **70**, pp. 1-50 (eds Duncan, R.A., D.K. Rea, J.K. Weissel, U. von Rad & R.B. Kidd), American Geophysical Union, Washington DC.

DICK, H.J.B., NATLAND, J.H. & MILLER, D.J. (Eds.). 1999. Proceedings of Ocean Drilling Program, Initial Reports (CD-ROM), Ocean Drilling Program, College Station, TX.

DICK, H.J.B., NATLAND, J.H., ALT, J.C., BACH, W., BIDEAU, D., GEE, J.S., HAGGAS, S., HERTOGEN, J.G.H., HIRTH, G., HOLM, P.M., ILDEFONSE, B., ITURRINO, G.J., JOHN, B.E., KELLET, D.S., KIKAWA, E., KINGDOM, A., LEROUX, P.J., MAEDE, J., MEYER, P.S., MILLER, D.J., NASLUND, H.R., NIU, Y., ROBINSON, P.T., SNOW, J., STEPHEN, R.A., TRIMY, P.W., WORM, H.U. & YOSHINOBU, A. 2000. A long in situ section of the lower ocean crust: results of ODP Leg 176 drilling at the Southwest Indian ridge. *Earth and Planetary Science Letters* **179**, 31-51.

DICK, H.J.B., OZAWA, K., MEYER, P.S., NIU, Y., ROBINSON, P.T., CONSTANTIN, M., HEBERT, R., MAEDA, J., NATLAND, J.H., HIRTH, G., MACKIE, S. 2002. Primary silicate mineral chemistry of a 1.5-km section of very slow spreading lower ocean crust: ODP Hole 735B, Southwest Indian Ridge. In *Proceedings of Ocean Drilling Program, Scientific Results* **176** (eds

Natland J.H., H.J.B. Dick, D.J. Miler, R. Von Herzen R.), pp. 1–60. Ocean Drilling Program, College Station, TX.

DICK, H.J.B., TIVEY, M.A. & TUCHOLKE, B.E. 2008. Plutonic foundation of a slow-spreading ridge segment: Oceanic core complex at Kane Megamullion. *Geochemistry Geophysics Geosystems* **9**, doi:1029/2007GC001645.

DOSSO, L., BOUGAULT, H., BEUZART, P., CALVEZ, J.-Y., JORON, J,-L. 1988. The geochemical structure of the South-East Indian Ridge. *Earth and Planetary Science Letters* **88**, 47–59

DROLIA, R.K., IYER, S.D., CHAKRABORTY, B., KODAGALI, V., RAY, D., MISRA, S., ANDRADE, R., SARMA, K.V.L.N.S., RAJASEKHAR, R.P. & MUKHOPADHYAY, R. 2003. The Northern Central Indian Ridge: Geology and tectonics of fracture zones-dominated spreading ridge segments. *Current Science* **85**, 290-298.

DROLIA, R.K. & DEMETS, C. 2005. Deformation in the diffuse India-Capricorn-Somalia triple junction from a multibeam and magnetic survey of the northern Central Indian ridge, 3°S-10°S. *Geochemistry Geophysics Geosystems* **6 (9)**, doi 10.1029/2005GC00950.

DUPRÉ, B. & ALLÈGRE, C.J. 1983. Pb–Sr isotope variations in Indian Ocean basalts and mixing phenomena. *Nature* **303**, 142–146.

ELTHON, D., CASEY, J.F. & KOMOR, S. 1982. Mineral chemistry of ultramafic cumulates from the North Arm Mountain massif of the Bay of Islands ophiolite: evidence for high-pressure crystal fractionation of oceanic basalts. *Journal of Geophysical Research* **87**, 8717–8734.

ELTHON, D. 1987. Petrology of gabbroic rocks from the Mid-Cayman rise spreading center. *Journal of Geophysical Research* **92**, 658-682.

ENGEL, C.G. & FISHER, R.L. 1975. Granitic to ultramafic rock complexes of the Indian ocean ridge system, Western Indian Ocean. *Bulletin Geological Society of America* **82**, 553-562.

FAURE, G. & MENSING, T. M. 2005. Isotopes- principles and applications (3rd edition), Wiley, 897 pp.

FRÜH-GREEN, G.L., PLAS, A., DELL'ANGELO, L.N. 1996. Mineralogic and stable isotope record of polyphase alteration of upper crustal gabbros of the pacific rise (Hess Deep, Site 894). In Proceedings Ocean Drilling Program, Scientific Results 147, (eds Mevel, C., K.M. Gillis, J.F. Allan and P.S. Meyer), pp. 235-254. Ocean Drilling Program, College Station, TX.

GALER, S.J.G. & ABOUCHAMI, W., 1998. Practicial application of lead triple spiking for correction of instrumental mass discrimination. *Mineralogical Magazine* **62A**, 491-492.

GAO, Y., SNOW, J.E., HELLEBRAND, E., VON DER HANDT, A., DICK, H. & HOEFS, J. 2003. Petrology of gabbros from Gakkel ridge, Geophysical Research Abstracts 5, 14591.

GURENKO, A.A. & SOBOLEV, A.V., 2006. Crust-primitive magma interaction beneath neovolcanic rift zone of Iceland recorded in gabbro xenolith from Midfell, SW Iceland. *Contributions to Mineralogy and Petrology* **151**, 495-520.

HANAN, B.B., BLICHERT-TOFT, J., PYLE, D.G. & CHRISTIE, D.M. 2004. Contrasting origins of the upper mantle revealed by hafnium and lead isotopes from the Southeast Indian Ridge. *Nature* **432**, 91–94.

HART, S.R. 1984. A large-scale isotope anomaly in the Southern Hemisphere mantle. *Nature* **309**, 753-757.

HART, S.R., BLUSZTAJN, J., DICK, H.J.B., MEYER, P.S. & MUEHLENBACH, K. 1999. The fingerprint of seawater circulation in a 500-meter section of ocean crust gabbros. *Geochimica Cosmochimica Acta* **63**, 4059-4080.

HEBERT, R., CONSTANTIN, M. & ROBINSON, P.T., 1991. Primary mineralogy of Leg 118 gabbroic rocks and their place in the spectrum of oceanic mafic igneous rocks. In *Proceedings Ocean Drilling Program, Scientific Results* **118** (eds Von Herzen, R.P., P.T. Robinson et al.), pp. 3-20. Ocean Drilling Program, College Station, TX.

HEBERT, R.D., BIDEAU, D. & HEKINIAN, R. 1983. Ultramafics and mafic rocks from the Garret transform fault near 13°30'S on the East Pacific Rise: Igneous Petrology. *Earth and Planetary Science Letters* **65**, 107-125.

ILDEFONSE, B., BLACKMAN, D.K., JOHN, B.E., OHARA, Y., MILLER, D.J., MACLEOD, C.J. & INTEGRATED DRILLING PROGRAM EXPEDITIONS 304/305 SCIENCE PARTY. 2007. Oceanic core complexes and crustal accretion at slow-spreading ridges. *Geology* **35**, 623-626.

IRVINE, T.N. 1982. Terminology for layered intrusions. *Journal of Petrology* **23**, 127-162.

KEMPTON, P.D., PEARCE, J.A., BARRY, T.L., FITTON, J.G., LANGMUIR, C. & CHRISTIE, D.M. 2002. Sr–Nd–Pb–Hf isotope results from ODP Leg 187: evidence for mantle dynamics of the Australian– Antarctic Discordance and origin of the Indian MORB source. *Geochemistry Geophysics Geosystems* **3**, doi: 10.1029/2002GC000320.

KURZ, M.D., LE ROEX, A. P, & DICK, H., 1998. Isotope geochemistry of the mantle beneath the Bouvet Triple Junction. *Geochimica Cosmochimica Acta* **62**, 841–852.

KURZ, M.D., WARREN, J.M.& CURTICE, J. 2009. Mantle deformation and noble gases: Helium and neon in oceanic mylonites. *Chemical Geology* **266**, 10-18.

LANGMUIR, C.H., VOCKE, JR. R.D., HANSON, G.N. & HART, S.H. 1978. A general mixing equation with applications to Icelandic basalts. *Earth and Planetary Science Letters* **37**, 380-392.

LANGMUIR, C.H. 1989. In-situ fractional crystallization. *Nature* **342**, 512-515.

LINDSLEY, D.H. 1981. Pyroxene thermometry. *American Mineralogist* **68**, 477-493.

LISSENBERG, C.J. & DICK, H.J.B. 2008. Melt-rock reaction in the lower oceanic crust and its implications for the genesis of mid-ocean ridge basalt. *Earth and Planetary Science Letters* **271**, 311-325.

MAHONEY, J.J., NATLAND, J.H., WHITE, W.M., POREDA, R., BLOOMER, S.H., FISHER, R.L. & BAXTER, A.N. 1989. Isotopic and geochemical provinces of the western Indian Ocean spreading centers. *Journal of Geophysical Research* **94**, 4033-4052.

MCDONOUGH, W.F. & SUN, S.S. 1995. The composition of the Earth. *Chemical Geology* **120**, 223-253.

MEYER, P.S., DICK, H.J.B. & THOMPSON, G. 1989. Cumulate gabbros from the Southwest Indian Ridge, 54ºS-7º16'E: implications for magmatic processes at a slow spreading ridge. *Contributions to Mineralogy and Petrology* **103**, 44-63.

MEYZEN, C.M., BLICHERT-TOFT, J., LUDDEN, J.N., HUMLER, E., MEVEL, C. & ALBAREDE, F., 2007. Isotopic portrayal of the earth's upper mantle flow field. *Nature* **447**, 1069-1074.

MICHARD, A., MONTIGNY, R. & SCHLICH, R. 1986. Geochemistry of the mantle beneath the Rodriguez triple junction and the South-East Indian Ridge. *Earth and Planetary Science Letters* **78**, 104-114.

MIYASHIRO, A. & SHIDO, F. 1980. Differentiation of gabbros in the mid-Atlantic ridge near 24ºN. *Geochemical Journal* **14**, 145-154.

MORISHITA, T., HARA, K., NAKALURA, K., SAWAGUCHI, T., TAMURA, A., ARAI, S., OKINO, K., TAKAI, K. & KUMAGAI, H. 2009. Igneous, alteration and exhumation processes recorded in abyssal peridotites and related fault rocks from an oceanic core complex along the Central Indian Ridge. *Journal of Petrology* **50**, 1299-1325.

NAKAMURA, K., SATO, H., SATO, Y. & ISHII, T. 2006. Petrological and geochemical study of the Indian Ocean MORB from the Rodriguez Triple Junction, Indian Ocean. American Goephysical Union Fall Meeting, #B31-B-1104

NOBRE SILVA, I.G., WEIS, D., BARLING, J. & SCOATES, J.S. 2009. Leaching systematics and matrix elimination for the determination of high-precision Pb-isotope compositions of ocean island basalts. *Geochemistry Geophysics Geosystems* **10**, doi 10.1029/2009GC002537.

PLUGER W.L., CRUISE PARTICIPANTS 1989. Fahrtbericht SO-28 and Wissenschaftlicher Bericht GEMINO-I: Geothermal Metallogenesis Indian Ocean, 274pp.

POUCHOU, J.-L. & PICHOIR, F. 1988. A simplified version of the "PAP" model for matrix correction in EPMA. In *Microbeam analyses 1988* (eds D.E. Newbury), pp 315-318, San Francisco Press, San Francisco, California.

PRESNALL, D.C. & HOOVER, J.D. 1987. High pressure phase equilibrium constraints on the origin of mid-ocean ridge basalts, In *Magmatc Processes: Physicochemical principles*, Geophysical Monograph, 71, pp. 75-89, (ed. Mysen, B.O.), AGU, Wasginton DC.

PRICE, R.C., KENNEDY, A.K., RIGGS-SNEERINGER, M. & FREY, F.A. 1986. Geochemistry of basalts from the Indian ocean triple junction: implications for the generation and evolution of Indian Ocean ridge basalts. *Earth and Planetary Science Letters* **78**, 379-396.

RAY, D., IYER, S.D., BANERJEE, R., MISRA, S. & WIDDOWSON, M. 2007. Petrology and Geochemistry of basalts from the Northern Central Indian Ridge (3-11ºS): implications for the evolution of MORB. *Acta Geologica Sinica (English edition)* **81**, 99-112.

REHKAMPER, M. & HOFMANN, A.W. 1997. Recycled ocean crust and sediment in Indian Ocean MORB. *Earth and Planetary Science Letters* **147**, 93-106.

RIDLEY, W.L. PERFIT, M.R. SMITH, M.C. & FORNARI, D.J. 2006. Magmatic processes in developing oceanic crust revealed in a cumulate xenolith collected at the East Pacific Rise, 9º50'N. *Geochemistry Geophysics Geosystems* **7**, doi:10.1029/2006GC001316

SHIPBOARD SCIENTIFIC PARTY. 2004. Leg 209 Summary, In *Proceeding Ocean Drilling Program Initial Reports* **209** (eds Kelemen, P.B., E. Kikawa and D.J. Miller DJ), pp. 1-139, Ocean Drilling Program, College Station, TX.

SUBBARAO, K.V. & HEDGE, C.E. 1973. K, Rb, Sr and $^{87}Sr/^{86}Sr$ in rocks from the Mid-Indian Ocean Ridge. *Earth and Planetary Science Letters* **18**, 223-228.

SUN, S.S. & MCDONOUGH, W.F. 1989. Chemical and isotope systematics of ocean basalts: implications for mantle composition and processes. In *Magmatism in the Ocean Basins* (eds Saunders, A.D. and M.J. Norry), pp. 313-345. Geological Society of London Special Publication, London, Special Publication no 42.

TAYLOR, S.R. & MCLENNAN, S.M. 1985. The continental crust: its composition and evolution, Blackwell Science Publication, 312 pp.

TIEZZI, L.J. & SCOTT, R.B. 1980. Crystal fractionation in a cumulate gabbro, Mid-Atlantic Ridge, 26ºN. *Journal of Geophysical Research* **85**, 5438-5454.

THY, P. 2003. Igneous petrology of gabbros from Hole 1105A: oceanic magma chamber processes. In *Proceeding Ocean Drilling Program, Scientific Results* **179** (eds Casey, J.F. and D.J. Miller), pp. 1-76. Ocean Drilling Program, College Station, TX.

TREUIL, M. & VARET, J. 1973. Critères volcanologiques, pètrologiques et gèchimiques de la genèse et de la différenciation des magmas basaltiques: example de l'Afar. *Bulletin Society of Geologique France* **15**, 401-644.

VANKO, D.A. & BATIZA, R. 1980. Gabbroic rocks from the Mathematician Ridge failed rift. *Nature* **300**, 742-744.

VILLIGER, S., ULMER, P., MUNTENER, O. & THOMPSON, A.B. 2004. The liquid line of descent of anhydrous, mantle derived, tholeiitic liquids by fractional and equilibrium crystallization-an experimental study at 1.0 GPa. *Journal of Petrology* **45**, 2369-2388.

VILLEMANT, B., JAFFREZIC, H., JORON, J.L. & TREUIL, M. 1981. Distribution coefficients of major and trace elements; fractional crystallization in the alkali basalt series of Chaine des Puys (Massif Central, France). *Geochimica Cosmochimica Acta* **45**, 1997-2016.

WALKER, D. SHIBATA, T. & DELONG, S.E. 1979. Abyssal tholeiites from the Oceanographer fracture zone II: Phase equillibria and mixing. *Contributions to Mineralogy and Petrology* **70**, 111-125.

WALKER, D. & DELONG, S.E. 1984. A small Soret effect in spreading center gabbros. *Contributions to Mineralogy and Petrology* **85**, 203-208.

WEIS, D. & FREY, F.A. 1996. Role of the Kerguelen plume in generating the eastern Indian Ocean seafloor. *Journal of Geophysical Research* **101(B6)**, 13381-13849.

WEIS, D., KIEFFER, B., MAERSCHALK, C., PRETORIUS, W. & BARLING, J. 2005. High-

precision Pb-Sr-Nd-Hf isotopic characterization of USGS BHVO-1 and BHVO-2 reference materials. *Geochemistry Geophysics Geosystems* **6**, Q02002, doi:10.1029/2004GC000852.

WEIS, D., KIEFFER, B., MAERSCHALK, C., BARLING, J., DE JONG, J., WILLIAMS, G.A., HANANO, D., PRETORIUS, W., MATTIELLI, N., SCOATES, J.S., GOOLAERTS, A., FRIEDMAN, R.M. & MAHONEY, J.B. 2006. High-precision isotopic characterization of USGS reference materials by TIMS and MC-ICP-MS. *Geochemistry Geophysics Geosystems* **7**, Q08006, doi:10.1029/ 2006GC001283.

WEIS, D., KIEFFER, B., HANANO, D., SILVA, I.N., BARLING, J., PRETORIUS, W., MAERSCHALK, C., & MATTIELLI, N. 2007. Hf isotope compositions of U.S. Geological Survey reference materials. *Geochemistry Geophysics Geosystems* **8**, Q06006, doi:10.1029/2006GC001473.

WHITE, W.M.1999. Trace elements in igneous processes, In *Encyclopedia of Earth Sciences* (ed Dasch, E. J.), pp. 256-307. U.S.A., Macmillan.

WINTER, J.D. 2001. A introduction to Igneous and Metamorphic Petrology, Prentice Hall, New Jersey, 697pp.

WORKMAN, R.K. & HART, S.R. 2005. Major and trace element composition of the depleted MORB mantle (DMM). *Earth and Planetary Science Letters* **231**, 53-72.

Table Captions

Table 1. Modal analyses of NCIR gabbro.

Table 2. Comparative average chemistry of plagioclase, clinopyroxene and olivine of NCIR gabbro, NCIR basalt and CIR gabbro.

Table 3. Major oxides, trace element and Sr, Pb and Nd isotopic data of the NCIR gabbros, the available chemical data of the CIR gabbros and NCIR basalts are given for comparison.

Figure Captions

Fig. 1. (a) Sketch map of Indian Ocean showing position of Indian Ocean Ridge System (IORS) (1), 90^{o}E ridge (2), and Sunda-Banda trench (3); (b) enlarged view of the box area in figure 1a showing multibeam map of the "Vityaz megamullion" (after Drolia and DeMets, 2005). Dredge location has been shown as DR 14. Symbols: CR-Carlsberg Ridge, CIR-Central Indian Ridge, RTJ-Rodriguez triple junction, SWIR-South West Indian Ridge and SEIR-South East Indian Ridge.

Fig. 2. Photomicrographs of Vityaz gabbros: (a) Olivine gabbro in plane polarized light showing ophitic or subophitic texture, note interstitial olivine (Ol) and clinopyroxene (Cpx) within plagioclase (Plag) grains that are in mutual contact, bar scale: 1 mm; (b) Plagioclase in olivine gabbro showing triple junction; (c) Digested plagioclase (Plag) within interstitial clinopyroxene (Cpx); (d) BSE image of Fe-Ti oxide gabbro showing subhedral equant Fe-Ti oxides. Bar scale for figs b, c and d are 0.5 mm.

Fig. 3. Plots of clinopyroxenes of NCIR gabbros in molar wollastonite (Wo)-enstatite (En)-ferrosilite (Fs) (i.e., pyroxene) ternary diagram, data from Appendix, Table A3. The pyroxene compositions obtained during fractional and equilibrium crystallization experiments on primitive mantle-derived tholeiitic basalt at 1.0 GPa (Villiger et al., 2004) and unpublished clinopyroxene data of NCIR basalts of first author (D. R.) are also shown for comparison; Symbols as in legend. Coexisting clinopyroxene and orthopyroxene compositions of Villiger et al. (2004) are connected with tie lines.

Fig. 4. Binary plots for mineral chemical compositions of NCIR gabbro: (a) Plagioclase in An (wt%) versus FeO_{total} (wt%) plot, (b) clinopyroxene in Mg# versus Al (a.p.f.u.) (atomic power formula unit) plot, (c) clinopyroxene in Mg# versus Cr (a.p.f.u.) plot, and (d) TiO_2 versus Cr_2O_3 plot (after Lissenberg and Dick, 2008) showing clinopyroxenes of NCIR gabbro are in equilibrium with melt that co-exists with mantle peridotite. Symbols: filled grey circle- plagioclase/pyroxene from olivine gabbro, filled black circle- plagioclase/pyroxene from oxide gabbro (Data from Appendix, Table A2 and A3), filled grey square- plagioclase/pyroxene from CIR gabbro (Bloomer et al., 1989) for comparison.

Fig. 5. Plot of primary and fractionated NCIR basalts (data from Ray et al., 2007 and our unpublished data), and NCIR olivine- and oxide gabbro (data from Table 3) in CIPW normative Olivine (Ol)-Diopside (Di)-Quartz (Qz) diagram projected from plagioclase apex (after Walker et al., 1979). Symbols: filled grey triangle- NCIR primary basalt, open square- NCIR basalt, filled grey circle-

olivine gabbro and filled black circle- oxide gabbro.

Fig. 6. Binary major oxide plots for NCIR gabbro and basalt in Mg# versus (a) SiO_2, (b) Al_2O_3, (c) CaO, (d) Na_2O and (e) P_2O_5, and (f) MgO versus TiO_2 plots; Mg#: mole Mg/ (mole Mg+ mole Fe^{2+}); Symbols: filled grey circle- olivine gabbo, filled black circle- oxide gabbro (data from Table 3), open square-NCIR basalt (Ray et al., 2007 and unpublished data), filled grey diamond- CIR gabbro (Engel and Fisher, 1975) and filled grey triangle-primitive NCIR MORB (Pluger et al., 1989).

Fig. 7. Normalised multielement plot (normalized to chondrite, after McDonough and Sun, 1995) of NCIR gabbro (data from Table 3), average NCIR MORB (Ray et al., 2007) and Indian Ocean pelagic sediment (Carlo, 1993; sample no 1H-2, 145-150, Leg 136) are shown for comparison. Symbols: filled grey circle- olivine gabbro, filled black circle- oxide gabbro, open square- average NCIR N-MORB and black filled triangle-average pelagic sediment.

Fig. 8. Binary trace element plots of NCIR gabbro (data from Table 3) and basalt (Ray et al., 2007) in Mg# versus (a) Zr, (b) Y, (c) Cr and (d) Ni diagrams; Symbols as in figure 7, note differences in trends for gabbro (dotted best fit lines) and basalt (solid best fit lines).

Fig. 9. (a) Chondrite normalized (after McDonough and Sun, 1995) REE spiderdiagram of NCIR gabbro and other Indian Ocean rocks for comparison. Symbols: filled grey circle- olivine gabbro, filled black circle- oxide gabbro (data from Table 3), filled diamond- D mantle (Workman and Hart, 2005), cross-Indian ocean pelagic sediment (detail REE data from Ben Othman et al., 1989), open square- average NCIR MORB and grey-shaded area- the range of NCIR MORB (data from Ray et al., 2007); (b) Binary plot of total REE (ΣREE) versus Mg# for Indian ocean gabbro and basalts; Symbols: filled grey circle- olivine gabbro, filled black circle- oxide gabbro (data from Table 3), open square- NCIR MORB (data from Ray et al., 2007).

Fig. 10. (a, b) Binary plots of present gabbro and NCIR basalts in compatible (Zr) versus incompatible trace element (Ni and Cr) log-log diagrams (after Cocherie, 1986), (c) plot of incompatible trace element ratio (Zr/Y) against the least compatible element of the two (Zr) (Process identification plot, after White, 1999); Symbols: filled grey circle- NCIR gabbro (data from Table 3) and open square- NCIR basalts (Ray et al., 2007), arrows showing direction of compositional changes with increasing Zr.

Fig.11. Binary plots of present gabbro in (a) La/Ce_N versus $^{206}Pb/^{204}Pb$, (b) $^{208}Pb/^{204}Pb$ versus $^{206}Pb/^{204}Pb$, (c) $^{207}Pb/^{204}Pb$ versus $^{206}Pb/^{204}Pb$, (d) $^{207}Pb/^{204}Pb$ versus $^{143}Nd/^{144}Nd$, and (e) $^{87}Sr/^{86}Sr$ versus $^{206}Pb/^{204}Pb$ plots; Symbols: filled grey circle- olivine gabbro (data from Table 3), open square- Central Indian Ocean Ridge (CIR) basalts (Rehkamper and Hofmann, 1997), filled black square- Indian ocean pelagic sediments (Ben Othman et al., 1989), filled black circle- depleted mantle (Hart, 1984); dashed and solid lines through the data indicate mixing lines between depleted mantle and Indian Ocean pelagic sediment end members. Note that the IOR basalt and NCIR gabbro are always plotted on mixing lines between these two end members; the role of pelagic sediments is also found to be important in the genesis of gabbro. Northern Hemisphere Reference Line (NHRL) from Hart (1984) is shown in figure 11 (b, c) for reference.

Table 1. Modal analyses of NCIR Gabbro

Sample Number	Volume modal proportions (in %) of mineral phases			
	Plagioclase	Clinopyroxene	Olivine	Opaque oxides
Gabbro-1 (olivine gabbro)	58	31	10	trace
Gabbro-2 (olivine gabbro)	50	35	15	trace
Gabbro-3 (Fe-Ti oxide gabbro)	43	40	not present	17
Gabbro-4(Fe-Ti oxide gabbro)	42	38	not present	19
Gabbro-5 (olivine gabbro)	61	17	22	trace
Gabbro-6 (olivine gabbro)	62	21	16	trace

Table 2. Comparative average chemistry of plagioclase, clinopyroxene and olivine of NCIR gabbro, NCIR basalt and CIR gabbro.

Component (wt%)	Plagioclase				Clinopyroxene				Olivine			
	NCIR Gabbro[1]		CIR Gabbro[2]	NCIR Basalt[3]	NCIR Gabbro[1]		CIR Gabbro[2]	NCIR Basalt[3]	NCIR Gabbro[1]		CIR Gabbro[2]	NCIR Basalt[3]
	Olivine gabbro	Fe-Ti oxide gabbro	12	22	Olivine gabbro	Fe-Ti oxide gabbro			Olivine gabbro	Fe-Ti oxide gabbro		
No. of grains analysed	9	9	12	22	8	7	19	6	8	8	9	15
SiO_2	50.17	51.33	49.78	48.38	51.66	52.56	52.65	45.51	39.44	39.32	39.81	41.09
TiO_2	0.06	0.08	0.06	0.03	0.35	0.39	0.53	2.7	0.01	0.01	0.08	0.02
Al_2O_3	31.16	30.54	32.78	31.95	3.53	2.64	2.84	8.085	0.02	0.01	0.01	0.14
CaO	14.27	13.12	15.37	16.52	20.66	20.72	20.90	21.66	0.14	0.08	0.08	0.29
FeO_t	0.3	0.43	0.41	0.3	5	6.43	5.32	10.41	18.42	20.02	17.28	13.23
MgO	0.1	0.19	0.12	0.22	16.90	16.56	17.35	10.24	42.71	39.85	43.7	43.79
Na_2O	3.43	3.91	2.68	2.28	0.32	0.33	0.30	0.43	0.01	0.02	0.01	0
K_2O	0.03	0.04	0.05	0.01	0.01	n.d.	0.02	0.02	n.d.	n.d.	0.01	0
MnO	0.01	0.03	0.01	0.06	0.13	0.21	0.18	0.15	0.28	0.28	0.30	0
P_2O_5	n.d.	0.01	n.a.	0	n.d.	n.d.	n.a.	n.d.	n.d.	n.d.	n.a.	0
NiO	0.02	0.02	n.a.	0	0.02	0.02	0.08	n.d.	0.11	0.15	0.17	0
Cr_2O_3	n.d.	0.02	n.a.	0	1.05	0.19	0.47	0.12	n.d.	0.01	0.05	n.d.
An	69.55	64.85	76	80.57	-		-	-	-	-	-	-
Ab	30.25	34.93	-	19.34	-		-	-	-	-	-	-
Or	0.2	0.21	-	0.1	-		-	-	-	-	-	-
Fo	-	-	-	-	-		-	-	80.52	78.02	82	85.47
Wo	-	-	-	-	42.96	42.5	42.49	49.25	-	-	-	-
En	-	-	-	-	48.90	47.22	49.07	32.16	-	-	-	-
Fs	-	-	-	-	8.14	10.28	8.44	18.59	-	-	-	-
Mg#	-	-	-	-	85.73	82.14	85.35	63	-	-	-	

Mg#= 100*mole Mg/ [mole (Mg+ mole Fe)]
n.d. not determined

1. Present StudyData from Appendix, tables A1, A2 and A3.
2. Data from Bloomer et al., 1989
3. Unpublished data of the D. Rayfirst author (D. Ray).

Table 3. Major oxides, trace element and Sr, Pb and Nd isotopic data of the NCIR gabbro, the available chemical data of the CIR gabbro and NCIR basalts are given for comparison.

	NCIR Gabbro							CIR Gabbro[1]	NCIR basalt[2]
Sample No.	Gabbro-1 (Ol. Gb.)	Gabbro-2 (Ol. Gb.)	Gabbro-5 (Ol. Gb.)	Gabbro-6 (Ol. Gb.)	Gabbro-3 (Fe-Ti Gb.)	Gabbro-4 (Fe-Ti Gb.)	Average olivine gabbro (n=4)		
Analysis no							4	5	41
SiO_2 (wt%)	48.28	48.01	47.42	48.69	47.44	47.35	48.10	48.94	48.66
TiO_2	0.17	0.16	0.15	0.21	2.61	0.45	0.17	1.57	1.40
Al_2O_3	17.15	16.23	14.04	15.38	11.63	13.07	15.70	15.83	15.36
Fe_2O_3	5.63	4.85	7.56	5.15	11.22	9.54	5.80	8.05	10.09
MnO	0.13	0.13	0.13	0.13	0.29	0.15	0.13	0.14	0.19
MgO	12.05	14.13	13.84	11.79	5.98	10.34	12.95	8.68	7.84
CaO	13.03	13.25	11.61	13.87	9.48	11.95	12.94	12.85	10.89
Na_2O	1.75	1.53	1.84	1.67	2.29	2.22	1.70	2.47	2.81
K_2O	0.03	0.02	0.03	0.03	0.06	0.06	0.03	0.10	0.27
P_2O_5	0.02	0.01	0.02	0.02	0.09	0.07	0.02	0.03	0.14
Mg#	81.0	85.0	78.0	82.0	51.0	68.0	80.33	68	59.0
Sc (ppm)	32	41	31	39.5	55	48.32	35.88	n.a.	35.11
V	108	144	105.5	117.1	373	217.44	118.65	n.a.	250
Cr	1316	1234	588.3	1819	65	190.33	1239.33	n.a.	268
Co	49	43.7	70	48	57	53.07	52.68	n.a.	86.05
Ni	229	192.08	254	22.8	29	121.16	174.47	n.a.	117.3
Cu	92	111	96	94	101	99.16	98.25	n.a.	82.2
Zn	19	18	24	20.32	147	36.26	20.33	n.a.	98.4
Ga	10	9.8	9.9	9.6	16	11.98	9.83	n.a.	16.44
Rb	0.5	0.4	0.6	0.5	0.7	0.89	0.50	n.a.	4.44
Sr	110	113.4	119	100	128.09	110	110.60	n.a.	136.13
Y	6	6.03	5	8.09	49.7	20	6.28	n.a.	32
Zr	10	4.8	7.3	13.7	90	24	8.95	n.a.	99.45
Nb	0.3	0.05	0.16	0.28	5.3	0.54	0.20	n.a.	4.16
Cs	0.02	0.02	0.014	0.01	0.05	0.03	0.02	n.a.	0.17
Ba	15	20.5	22.7	12.8	27.5	24	17.75	n.a.	40.02
La	0.5	0.3	0.4	0.51	2.2	1.42	0.43	n.a.	4
Ce	1.4	0.7	0.98	1.6	7.8	4.29	1.17	n.a.	12
Pr	0.2	0.1	0.15	0.26	1.4	0.69	0.18	n.a.	1.64
Nd	1.4	0.94	1.02	1.76	10.2	4.63	1.28	n.a.	10.41
Sm	0.5	0.5	0.4	0.66	4.06	1.76	0.52	n.a.	3.3
Eu	0.3	0.3	0.32	0.4	2.02	0.74	0.33	n.a.	1.21
Gd	0.8	0.6	0.6	0.92	5.5	2.27	0.73	n.a.	4.69
Tb	0.1	0.12	0.09	0.16	0.99	0.40	0.12	n.a.	0.85
Dy	0.9	0.95	0.74	1.3	7.7	3.07	0.97	n.a.	5
Ho	0.2	0.2	0.17	0.3	1.6	0.63	0.22	n.a.	1.06
Er	0.6	0.5	0.42	0.76	4.5	1.78	0.57	n.a.	3.35
Tm	0.07	0.06	0.05	0.09	0.59	0.22	0.07	n.a.	0.64
Yb	0.4	0.4	0.33	0.53	3.51	1.34	0.42	n.a.	3.11
Lu	0.1	0.08	0.07	0.12	0.8	0.29	0.09	n.a.	0.48
Hf	0.3	0.2	0.22	0.40	2.5	0.77	0.28	n.a.	n.d.
Th	0.1	0.03	0.05	0.06	0.08	0.10	0.06	n.a.	0.31
U	0.1	0.02	0.04	0.03	0.06	0.05	0.05	n.a.	0.13
$^{87}Sr/^{86}Sr$	0.702919 ±8		0.702878 ±6						0.702844±7[3]
$^{206}Pb/^{204}Pb$	18.4641 ±11		18.5316 ±17						18.067[3]
$^{207}Pb/^{204}Pb$	15.5392 ±11		15.5538 ±15						15.456[3]
$^{208}Pb/^{204}Pb$	38.3850 ±26		38.4593 ±53						37.870[3]
$^{143}Nd/^{144}Nd$	0.513119±19		0.513116 ±22						0.513081±10[3]

Olv. Gb.- Olivine gabbro, Fe-Ti Gb.- Fe-Ti oxide gabbro, n.a.- not available,

[1] Data from Engel and Fisher (1975) and Dmitriv and Sharaskin (1975)., [2] Ray et al. (2007), [3] Sample no 33 Dr (Table 1of Rehkamper and Hofmann, 1997).

Appendix

Table A1. Microprobe analyses of Olivine

	Fe-Ti oxide gabbro									Olivine gabbro							
	Gabbro-3a	Gabbro-3b	Gabbro-3c	Gabbro-3d	Gabbro-3e	Gabbro-3f	Gabbro-3g	Gabbro-3h		Gabbro-1a	Gabbro-1b	Gabbro-1c	Gabbro-1d	Gabbro-6a	Gabbro-6b	Gabbro-6c	Gabbro-6d
SiO_2	39.14	39.85	39.11	39.21	40.23	39.03	39.01	38.97		39.42	39.91	39.61	39.03	39.11	39.23	39.55	39.66
TiO_2	0.00	0.00	0.01	0.00	0.02	0.02	0.04	0.00		0.00	0.02	0.02	0.00	0.00	0.04	0.00	0.00
Al_2O_3	0.01	0.02	0.04	0.01	0.00	0.00	0.02	0.00		0.00	0.06	0.00	0.00	0.08	0.04	0.00	0.00
Cr_2O_3	0.00	0.00	0.00	0.02	0.04	0.01	0.03	0.00		0.00	0.00	0.01	0.00	0.00	0.00	0.02	0.00
FeOt	19.72	20.25	19.68	19.52	20.29	19.98	20.39	20.32		18.63	18.45	18.46	18.34	18.32	18.28	18.35	18.51
MnO	0.30	0.29	0.30	0.29	0.25	0.30	0.25	0.25		0.39	0.23	0.21	0.30	0.29	0.28	0.26	0.24
MgO	39.76	40.41	39.59	39.37	40.17	39.66	40.16	39.66		42.77	41.59	42.79	42.91	42.86	42.88	43.01	42.85
CaO	0.06	0.05	0.08	0.05	0.10	0.09	0.08	0.09		0.11	0.09	0.13	0.12	0.26	0.13	0.15	0.11
Na_2O	0.03	0.00	0.02	0.05	0.03	0.00	0.00	0.00		0.01	0.02	0.01	0.01	0.00	0.02	0.00	0.03
K2O	0.00	0.00	0.00	0.00	0.00	0.00	0.01	0.00		0.00	0.00	0.01	0.00	0.00	0.01	0.00	0.00
NiO	0.16	0.11	0.16	0.21	0.21	0.09	0.11	0.12		0.07	0.13	0.19	0.20	0.11	0.11	0.00	0.05
Total	99.19	100.98	98.98	98.74	101.34	99.19	100.11	99.40		101.40	100.50	101.44	100.91	101.03	101.02	101.34	101.45
Cations based on 4 oxygens																	
Si	1.014	1.014	1.015	1.019	1.02	1.012	1.004	1.01		0.994	1.012	0.998	0.989	0.991	0.992	0.996	0.998
Ti	0	0	0	0	0	0	0.001	0		0	0	0	0	0	0.001	0	0
Al	0	0.001	0.001	0	0	0	0.001	0		0	0.002	0	0	0.002	0.001	0	0
Cr	0	0	0	0	0.001	0	0.001	0		0	0	0	0	0	0	0	0
Fe	0.427	0.431	0.427	0.424	0.43	0.433	0.439	0.44		0.393	0.391	0.389	0.389	0.388	0.387	0.386	0.39
Mn	0.007	0.006	0.007	0.006	0.005	0.007	0.005	0.006		0.008	0.005	0.004	0.006	0.006	0.006	0.006	0.005
Mg	1.535	1.533	1.531	1.525	1.518	1.533	1.541	1.532		1.608	1.573	1.607	1.622	1.619	1.617	1.615	1.608
Ca	0.002	0.001	0.002	0.001	0.003	0.003	0.002	0.002		0.003	0.002	0.004	0.003	0.007	0.004	0.004	0.003
Ni	0.003	0.002	0.003	0.004	0.004	0.002	0.002	0.002		0.001	0.003	0.004	0.004	0.002	0.002	0	0.001
Fo	78.24	78.05	78.19	78.25	77.93	77.98	77.83	77.69		80.36	80.09	80.51	80.66	80.67	80.69	80.71	80.48

Table A2. Microprobe analyses of Plagioclase

	Fe-Ti gabbro										Olivine gabbro								
	Gabbro-3a	Gabbro-3b	Gabbro-3c	Gabbro-3d	Gabbro-3e	Gabbro-3f	Gabbro-3g	Gabbro-3h	Gabbro-3i		Gabbro-1a	Gabbro-1b	Gabbro-1c	Gabbro-1d	Gabbro-6a	Gabbro-6b	Gabbro-6c	Gabbro-6d	Gabbro-6e
SiO_2	50.87	51.22	50.57	51.66	51.45	51.35	51.54	51.39	51.90		50.46	50.08	50.68	50.62	51.24	50.22	50.56	48.88	48.75
TiO_2	0.19	0.06	0.10	0.07	0.02	0.07	0.08	0.04	0.06		0.06	0.12	0.04	0.09	0.00	0.08	0.07	0.11	0.00
Al_2O_3	30.95	30.59	30.89	30.97	30.64	30.21	30.04	30.23	30.37		31.13	31.09	30.74	30.89	30.94	30.66	31.14	31.73	32.14
Cr_2O_3	0.01	0.05	0.05	0.04	0.00	0.00	0.00	0.00	0.00		0.00	0.00	0.01	0.00	0.00	0.00	0.00	0.00	0.00
FeOt	0.25	0.25	0.40	0.40	0.45	0.77	0.42	0.49	0.41		0.26	0.33	0.27	0.38	0.29	0.29	0.31	0.27	0.30
MnO	0.09	0.05	0.01	0.00	0.01	0.02	0.01	0.00	0.05		0.00	0.02	0.03	0.00	0.00	0.02	0.00	0.00	0.00
MgO	0.09	0.00	0.08	0.03	0.05	1.29	0.04	0.05	0.05		0.07	0.10	0.10	0.08	0.10	0.10	0.12	0.10	0.10
CaO	13.01	13.35	13.83	13.53	13.43	12.73	12.85	12.59	12.79		14.13	14.03	13.73	13.85	13.89	14.04	14.29	15.14	15.37
Na_2O	3.57	3.55	3.57	3.99	4.03	3.91	4.05	4.25	4.26		3.68	3.58	3.58	3.68	3.68	3.46	3.43	2.94	2.86
K_2O	0.04	0.00	0.04	0.03	0.05	0.03	0.08	0.02	0.05		0.07	0.01	0.03	0.03	0.03	0.05	0.06	0.02	0.00
NiO	0.06	0.00	0.04	0.03	0.00	0.00	0.02	0.00	0.01		0.00	0.08	0.00	0.06	0.00	0.05	0.00	0.02	0.00
Cl	0.00	0.07	0.06	0.00	0.00	0.00	0.01	0.02	0.01		n.d.	n.d.	n.d.	n.d.	n.d.	n.d.	n.d.	n.d.	n.d.
P_2O_5	0.00	0.00	0.02	0.00	0.01	0.00	0.05	0.00	0.02		n.d.	n.d.	n.d.	n.d.	n.d.	n.d.	n.d.	n.d.	n.d.
Total	99.12	99.19	99.64	100.75	100.13	100.37	99.18	99.07	99.97		99.86	99.44	99.21	99.68	100.17	98.97	99.98	99.21	99.52
Cations based on 8 oxygens																			
Si	2.316	2.347	2.315	2.335	2.34	2.331	2.363	2.357	2.36		2.305	2.299	2.325	2.316	2.328	2.314	2.306	2.254	2.242
Ti	0.007	0	0.003	0.003	0.001	0.002	0.003	0.001	0.002		0.002	0.004	0.001	0.003	0	0.003	0.002	0.004	0
Al	1.687	1.652	1.667	1.65	1.643	1.617	1.623	1.635	1.628		1.676	1.683	1.663	1.666	1.657	1.666	1.674	1.725	1.742
Cr	0	0.002	0.002	0.001	0	0	0	0	0		0	0	0	0	0	0	0	0	0
Fe	0.01	0.009	0.015	0.015	0.017	0.029	0.016	0.019	0.016		0.01	0.013	0.01	0.015	0.011	0.011	0.012	0.01	0.012
Mn	0.004	0.002	0	0	0	0.001	0	0	0.002		0	0.001	0.001	0	0	0.001	0	0	0
Mg	0.006	0	0.006	0.002	0.003	0.087	0.003	0.003	0.003		0.005	0.007	0.007	0.005	0.007	0.007	0.008	0.007	0.007
Ca	0.645	0.655	0.679	0.655	0.654	0.619	0.631	0.619	0.623		0.692	0.69	0.675	0.679	0.676	0.693	0.698	0.748	0.757
Na	0.32	0.316	0.317	0.35	0.355	0.344	0.36	0.378	0.375		0.326	0.319	0.318	0.326	0.324	0.309	0.303	0.263	0.255
K	0.002	0	0.002	0.002	0.003	0.002	0.004	0.001	0.003		0.004	0.001	0.002	0.002	0.002	0.003	0.003	0.001	0
An	66.70	67.46	68.04	65.04	64.62	64.15	63.42	62.02	62.24		67.71	68.32	67.84	67.43	67.47	68.96	69.52	73.91	74.80
Ab	33.09	32.54	31.76	34.76	35.08	35.65	36.18	37.88	37.46		31.90	31.58	31.96	32.37	32.34	30.75	30.18	25.99	25.20
Or	0.21	0.00	0.20	0.20	0.30	0.21	0.40	0.10	0.30		0.39	0.10	0.20	0.20	0.20	0.30	0.30	0.10	0.00

Table A3. Microprobe analyses of Clinopyroxene

	Fe-Ti oxide gabbro								Olivine gabbro							
	Gabbro-3a	Gabbro-3b	Gabbro-3c	Gabbro-3d	Gabbro-3e	Gabbro-3f	Gabbro-3g		Gabbro-1a	Gabbro-1b	Gabbro-1c	Gabbro-1d	Gabbro-6a	Gabbro-6b	Gabbro-6c	Gabbro-6d
SiO_2	53.16	51.82	51.93	52.43	52.37	53.84	52.37		51.39	51.55	51.39	51.69	52.15	52.20	51.64	51.24
TiO_2	0.33	0.31	0.37	0.42	0.40	0.47	0.40		0.37	0.35	0.34	0.38	0.31	0.37	0.32	0.34
Al_2O_3	2.65	2.57	2.78	2.51	2.80	2.37	2.80		3.64	3.69	3.62	3.33	3.37	3.36	3.50	3.75
Cr_2O_3	0.16	0.24	0.17	0.18	0.18	0.19	0.18		1.06	1.02	1.04	1.03	0.82	1.08	1.01	1.30
FeOt	7.09	6.14	6.08	6.11	6.06	7.45	6.06		5.26	5.16	5.18	5.04	4.78	4.64	5.02	4.94
MnO	0.20	0.17	0.32	0.22	0.14	0.27	0.14		0.14	0.16	0.15	0.14	0.11	0.16	0.09	0.06
MgO	17.21	15.97	16.32	16.27	16.16	17.83	16.16		16.66	16.26	16.74	16.80	16.51	16.51	17.60	18.09
CaO	19.27	20.73	21.08	21.91	21.60	18.82	21.60		20.51	21.60	20.54	20.42	22.23	21.48	20.10	18.43
Na_2O	0.31	0.36	0.40	0.33	0.30	0.28	0.30		0.33	0.34	0.31	0.34	0.31	0.31	0.33	0.28
K_2O	0.01	0.00	0.01	0.00	0.00	0.00	0.00		0.00	0.00	0.00	0.00	0.03	0.01	0.00	0.00
NiO	0.06	0.03	0.00	0.03	0.00	0.00	0.00		0.04	0.00	0.01	0.02	0.00	0.03	0.00	0.09
Total	100.46	98.34	99.46	100.42	100.00	101.52	100.00		99.40	100.13	99.32	99.19	100.62	100.15	99.61	98.52
Cations based on 6 oxygens																
Si	1.94	1.936	1.921	1.924	1.925	1.943	1.925		1.890	1.884	1.890	1.903	1.894	1.906	1.887	1.891
Ti	0.009	0.009	0.01	0.012	0.011	0.013	0.011		0.010	0.010	0.009	0.011	0.009	0.010	0.009	0.009
Al	0.114	0.113	0.121	0.109	0.121	0.101	0.121		0.158	0.160	0.157	0.145	0.145	0.145	0.151	0.163
Cr	0.005	0.007	0.005	0.005	0.005	0.005	0.005		0.031	0.030	0.030	0.030	0.024	0.031	0.029	0.038
Fe	0.216	0.192	0.188	0.188	0.186	0.225	0.186		0.162	0.158	0.159	0.155	0.146	0.142	0.154	0.153
Mn	0.006	0.005	0.01	0.007	0.004	0.008	0.004		0.004	0.005	0.005	0.004	0.003	0.005	0.003	0.002
Mg	0.936	0.889	0.899	0.89	0.885	0.959	0.885		0.913	0.886	0.918	0.922	0.894	0.899	0.959	0.995
Ca	0.753	0.83	0.836	0.862	0.851	0.728	0.851		0.808	0.846	0.809	0.806	0.865	0.840	0.787	0.729
Na	0.022	0.026	0.029	0.024	0.021	0.02	0.021		0.024	0.024	0.022	0.024	0.022	0.022	0.023	0.020
Wo	39.53	43.43	43.47	44.43	44.28	38.08	44.28		42.91	44.76	42.90	42.80	45.41	44.66	41.42	38.84
En	49.13	46.52	46.75	45.88	46.05	50.16	46.05		48.49	46.88	48.67	48.96	46.93	47.79	50.47	53.01
Fs	11.34	10.05	9.78	9.69	9.68	11.77	9.68		8.60	8.36	8.43	8.23	7.66	7.55	8.11	8.15
Mg#	81.25	82.24	82.70	82.56	82.63	81.00	82.63		84.93	84.87	85.24	85.61	85.96	86.36	86.16	86.67

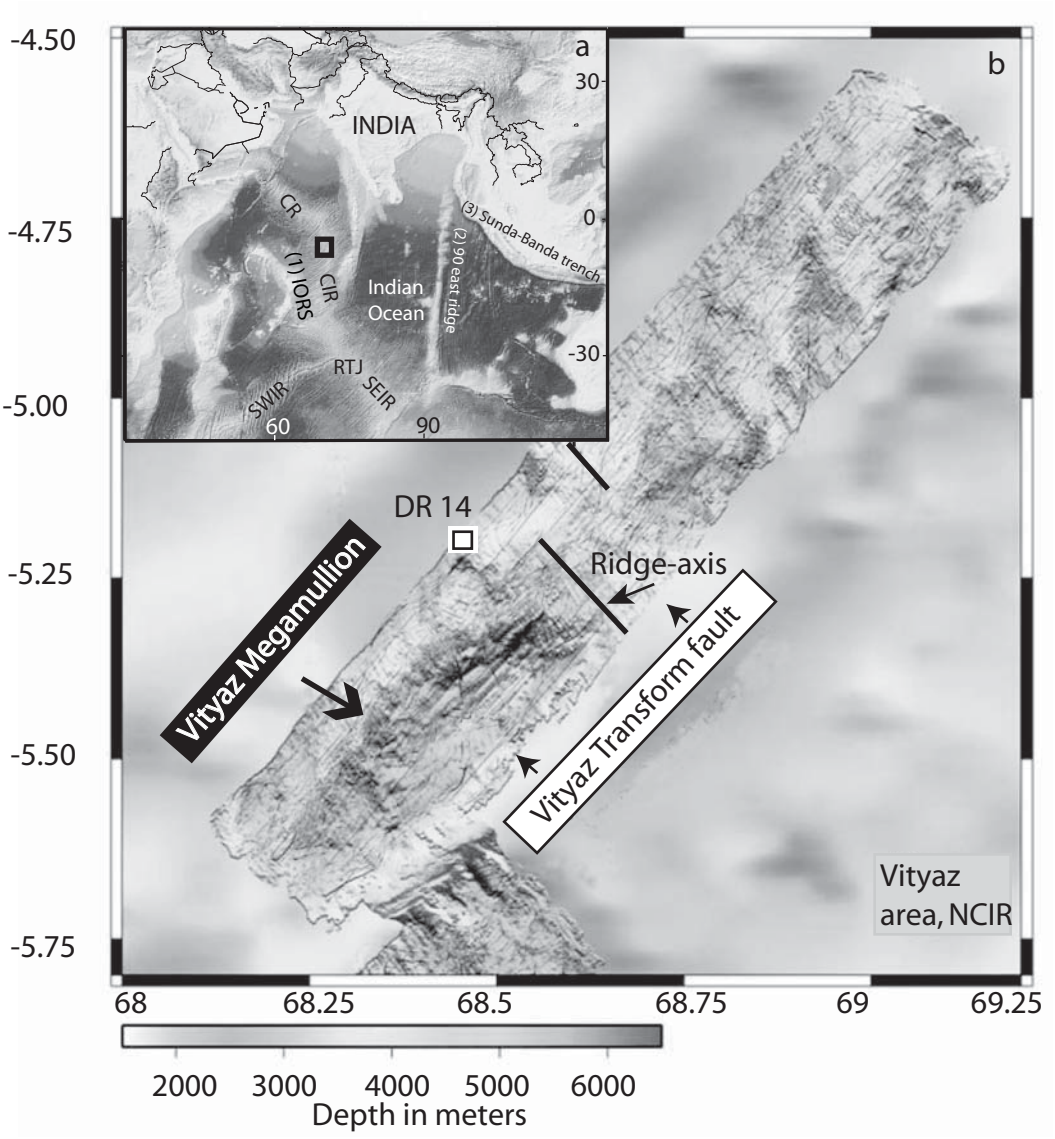
a
b
INDIA
CR
CIR
(1) IORS
Indian
Ocean
(2) 90 east ridge
(3) Sunda-Banda trench
RTJ
SWIR
SEIR
30
0
-30
60
90
DR 14
Ridge-axis
Vityaz Megamullion
Vityaz Transform fault
Vityaz
area, NCIR
-4.50
-4.75
-5.00
-5.25
-5.50
-5.75
68
68.25
68.5
68.75
69
69.25
2000
3000
4000
5000
6000
Depth in meters

Figure 1

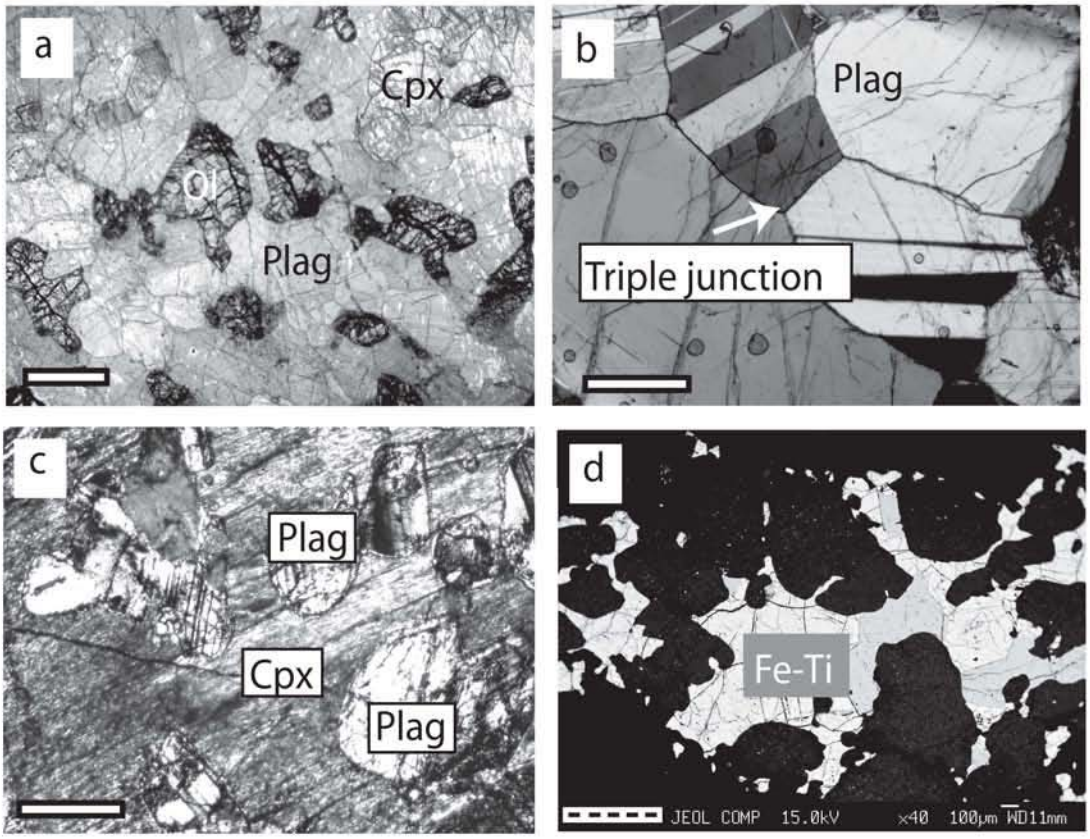
a
Cpx
Ol
Plag
b
Plag
Triple junction
c
Plag
Cpx
Plag
d
Fe-Ti
JEOL COMP 15.0kV ×40 100μm WD11mm

Figure 2

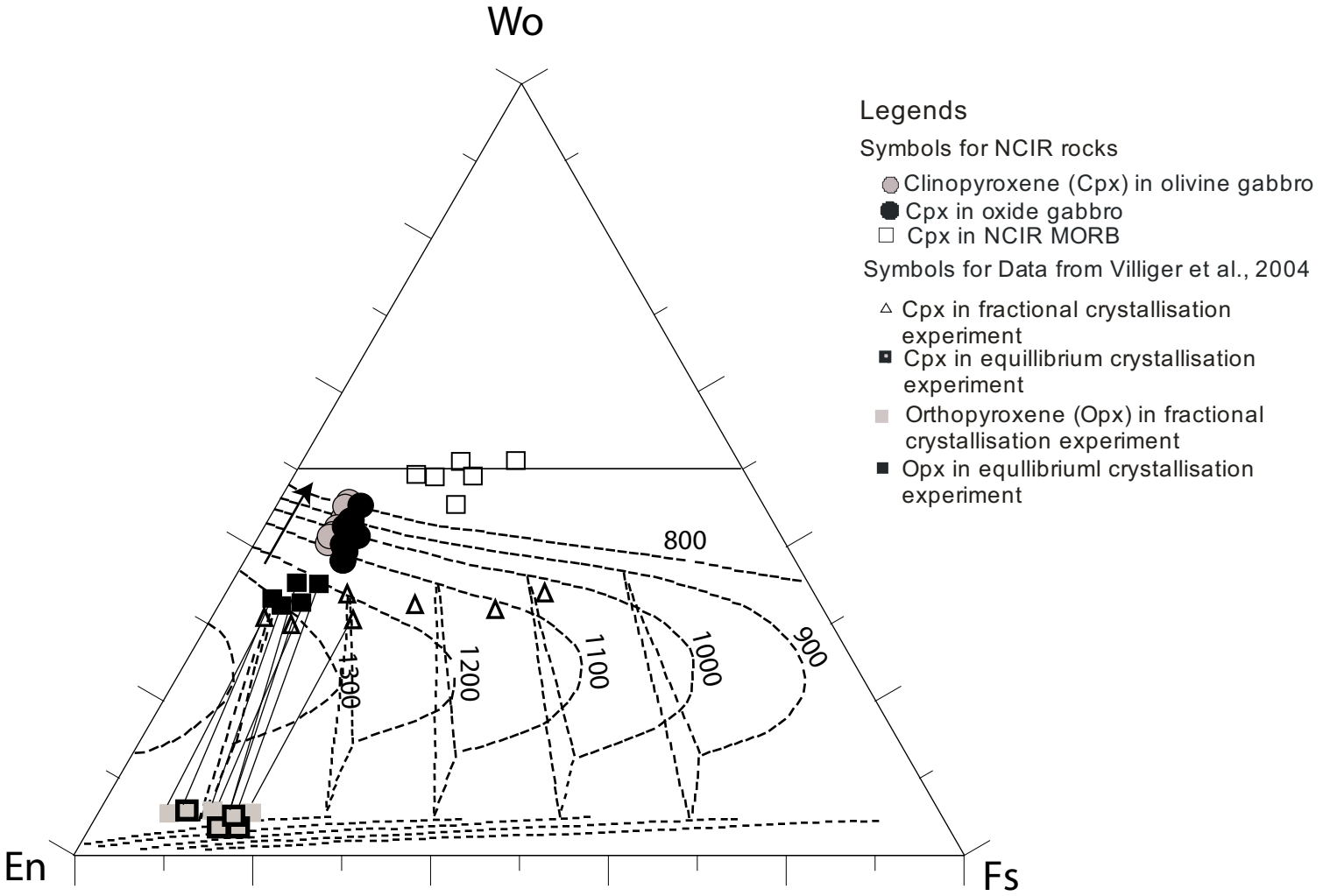
Wo
En
Fs
800
900
1000
1100
1200
1300
Legends
Symbols for NCIR rocks
Clinopyroxene (Cpx) in olivine gabbro
Cpx in oxide gabbro
Cpx in NCIR MORB
Symbols for Data from Villiger et al., 2004
Cpx in fractional crystallisation experiment
Cpx in equillibrium crystallisation experiment
Orthopyroxene (Opx) in fractional crystallisation experiment
Opx in equllibriuml crystallisation experiment

Figure 3

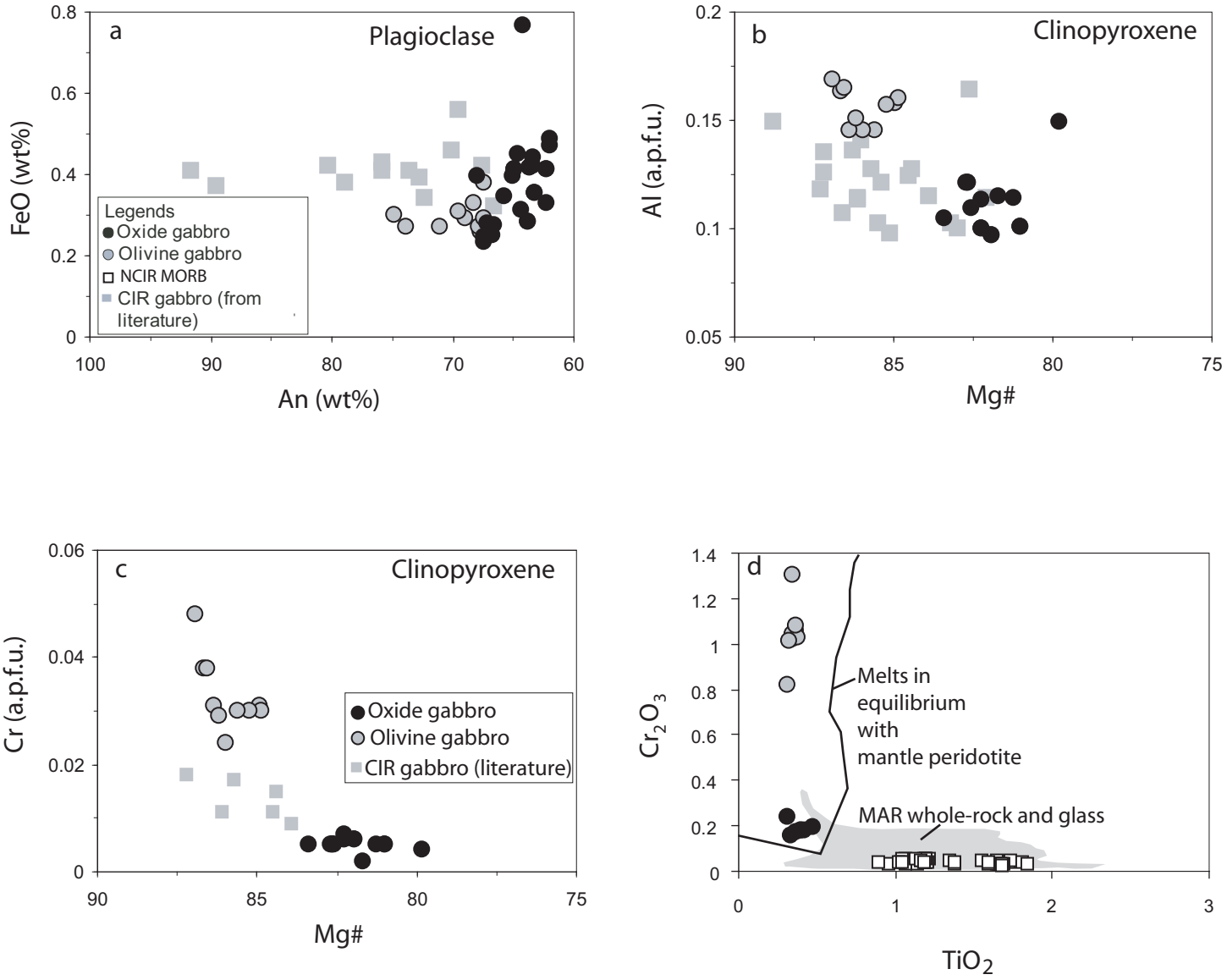
a
Plagioclase
FeO (wt%)
An (wt%)
Legends
Oxide gabbro
Olivine gabbro
NCIR MORB
CIR gabbro (from literature)
b
Clinopyroxene
Al (a.p.f.u.)
Mg#
c
Clinopyroxene
Cr (a.p.f.u.)
Mg#
Oxide gabbro
Olivine gabbro
CIR gabbro (literature)
d
Cr_2O_3
TiO_2
Melts in equilibrium with mantle peridotite
MAR whole-rock and glass

Figure 4

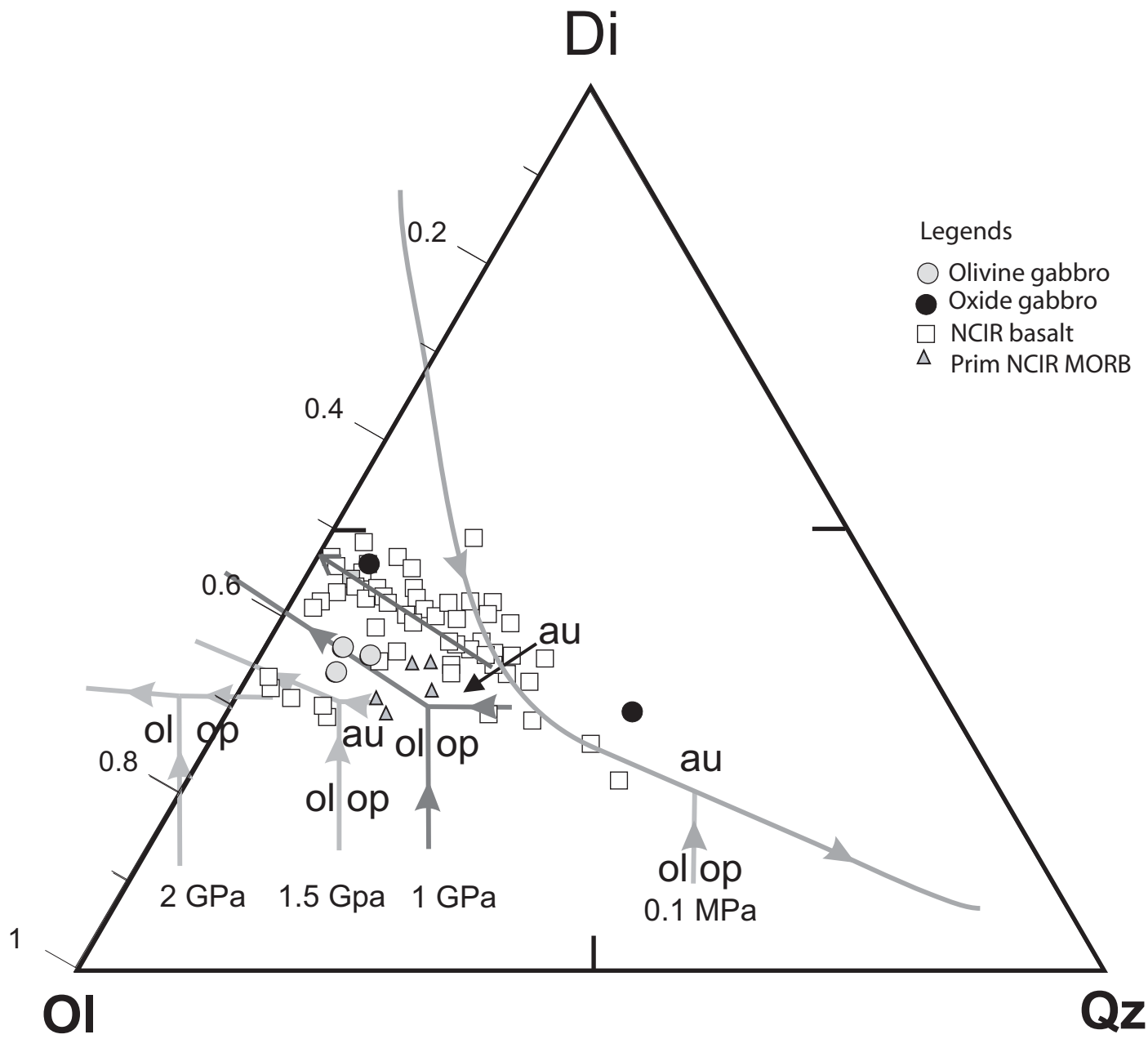
Di
0.2
0.4
0.6
0.8
1
Ol
Qz
Legends
Olivine gabbro
Oxide gabbro
NCIR basalt
Prim NCIR MORB
au
ol op
au
ol op
ol op
au
ol op
2 GPa
1.5 Gpa
1 GPa
0.1 MPa

Figure 5

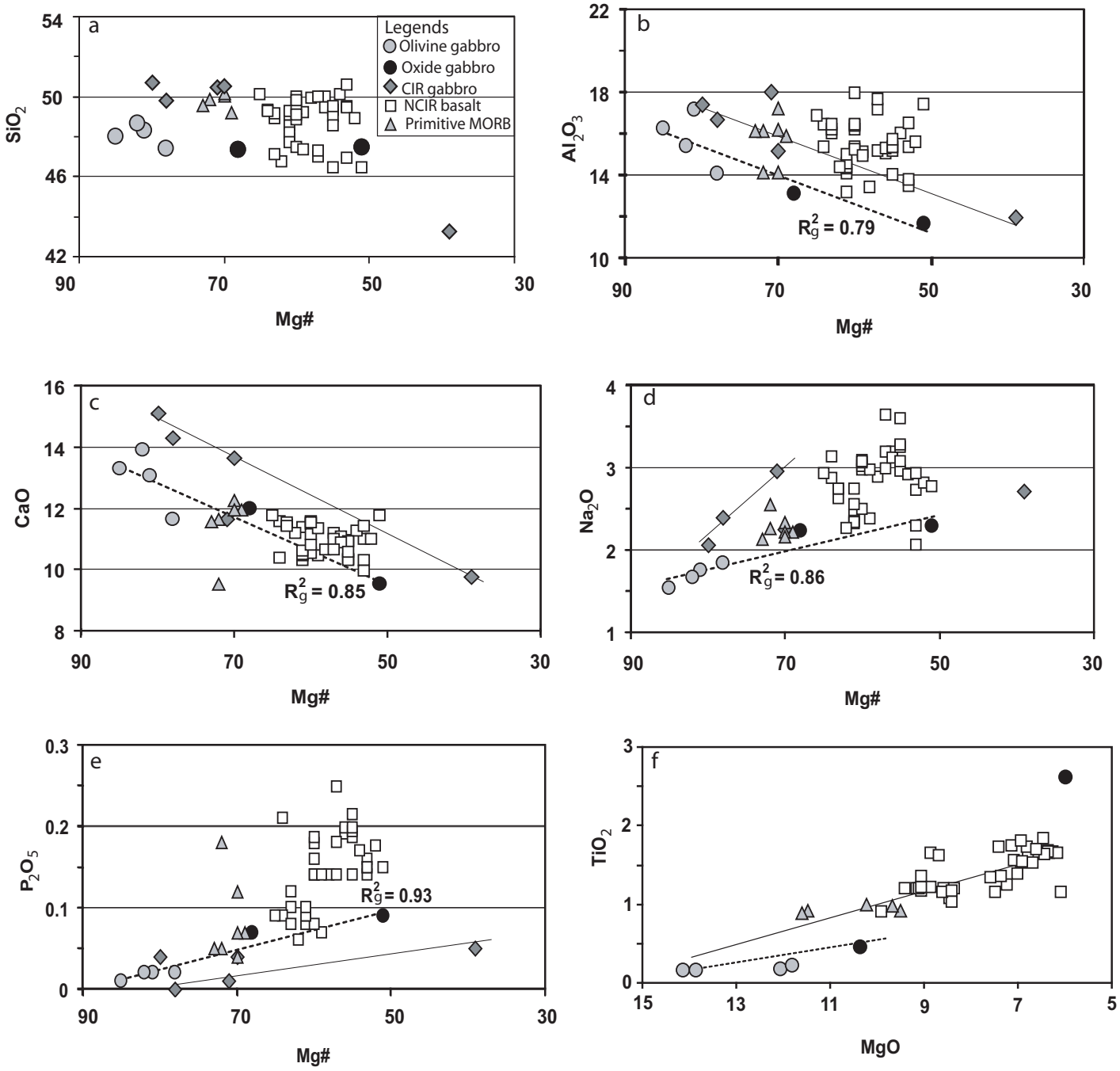
a
Legends
Olivine gabbro
Oxide gabbro
CIR gabbro
NCIR basalt
Primitive MORB
SiO2
Mg#
b
Al2O3
Rg2 = 0.79
c
CaO
Rg2 = 0.85
d
Na2O
Rg2 = 0.86
e
P2O5
Rg2 = 0.93
f
TiO2
MgO

Figure 6

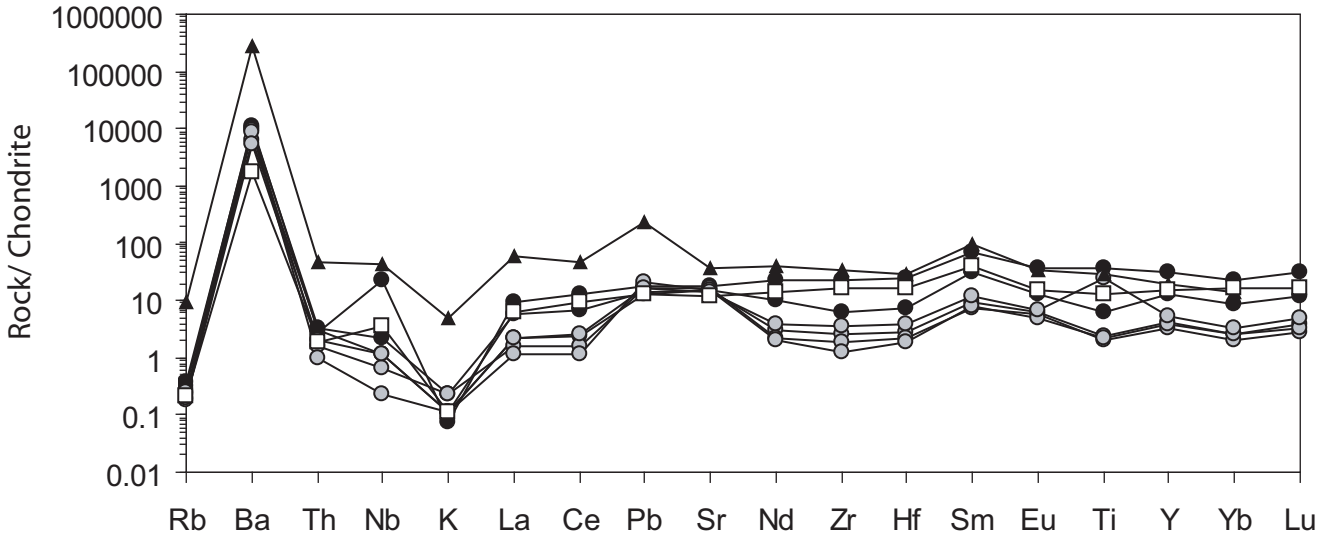
Rock/ Chondrite
1000000
100000
10000
1000
100
10
1
0.1
0.01
Rb
Ba
Th
Nb
K
La
Ce
Pb
Sr
Nd
Zr
Hf
Sm
Eu
Ti
Y
Yb
Lu

Figure 7

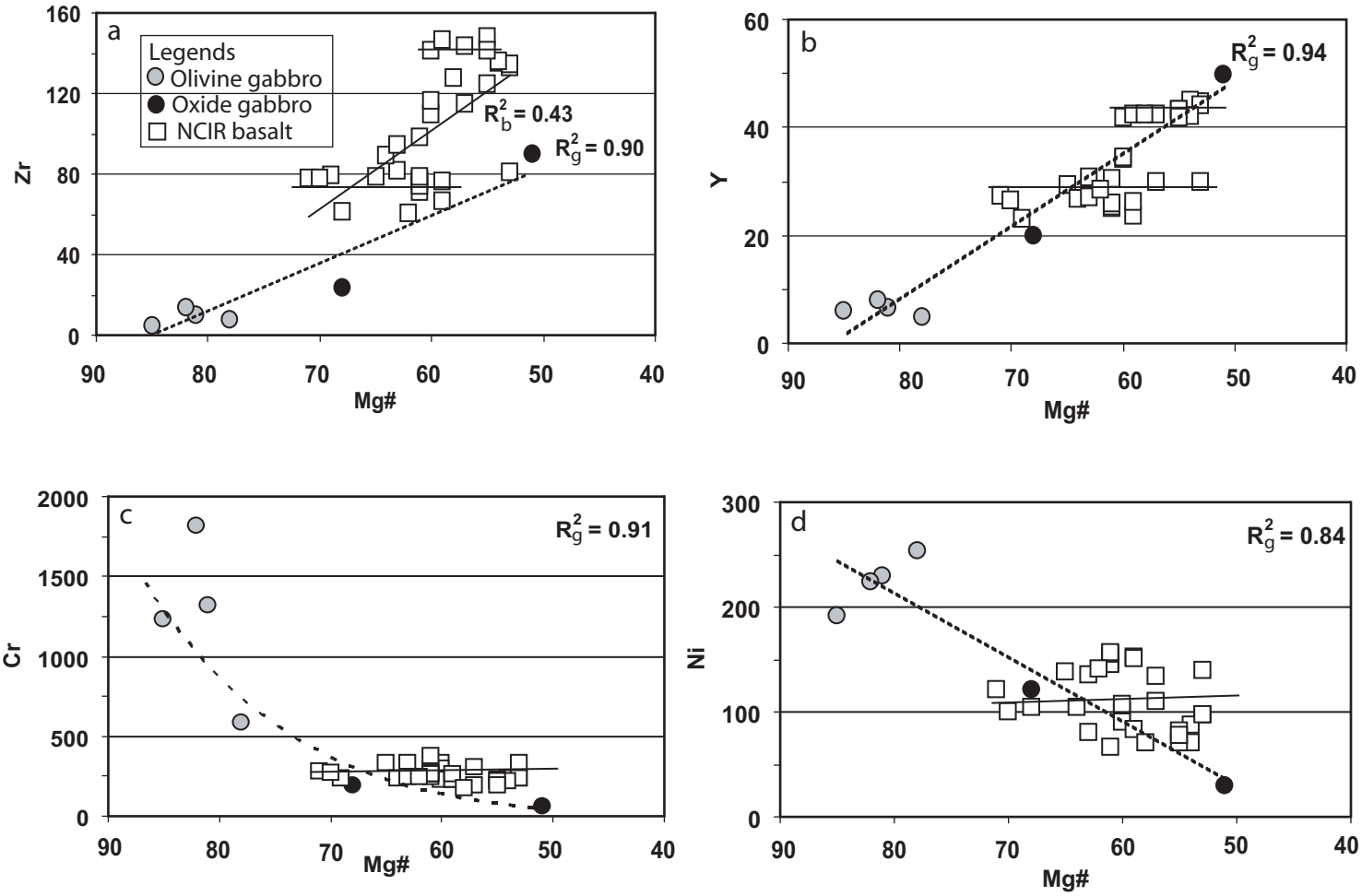
a
Legends
Olivine gabbro
Oxide gabbro
NCIR basalt
R_b^2 = 0.43
R_g^2 = 0.90
Zr
Mg#
b
R_g^2 = 0.94
Y
Mg#
c
R_g^2 = 0.91
Cr
Mg#
d
R_g^2 = 0.84
Ni
Mg#

Figure 8

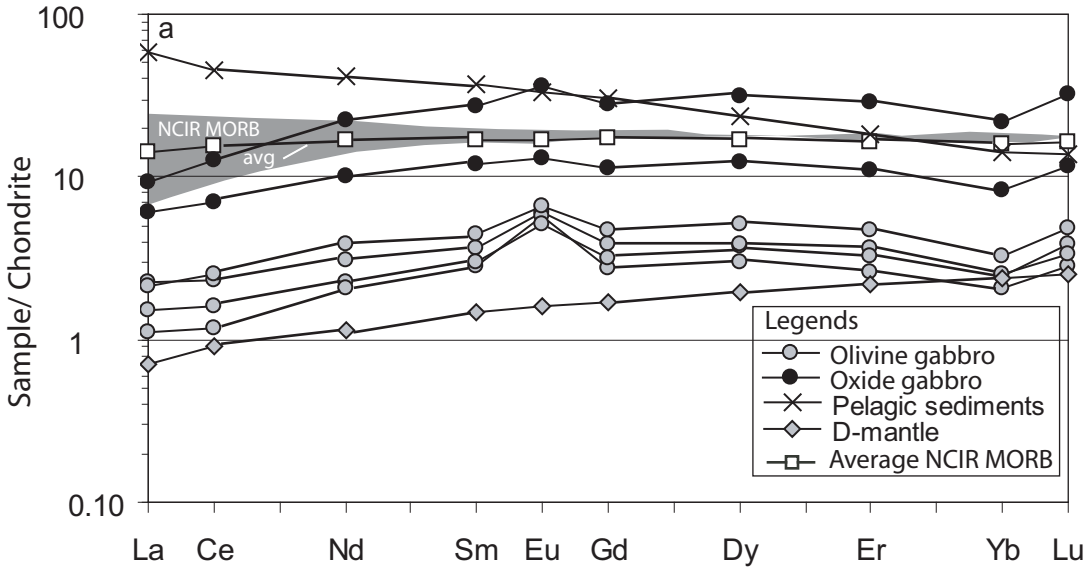
a
100
10
1
0.10
Sample/ Chondrite
NCIR MORB
avg
Legends
Olivine gabbro
Oxide gabbro
Pelagic sediments
D-mantle
Average NCIR MORB
La
Ce
Nd
Sm
Eu
Gd
Dy
Er
Yb
Lu

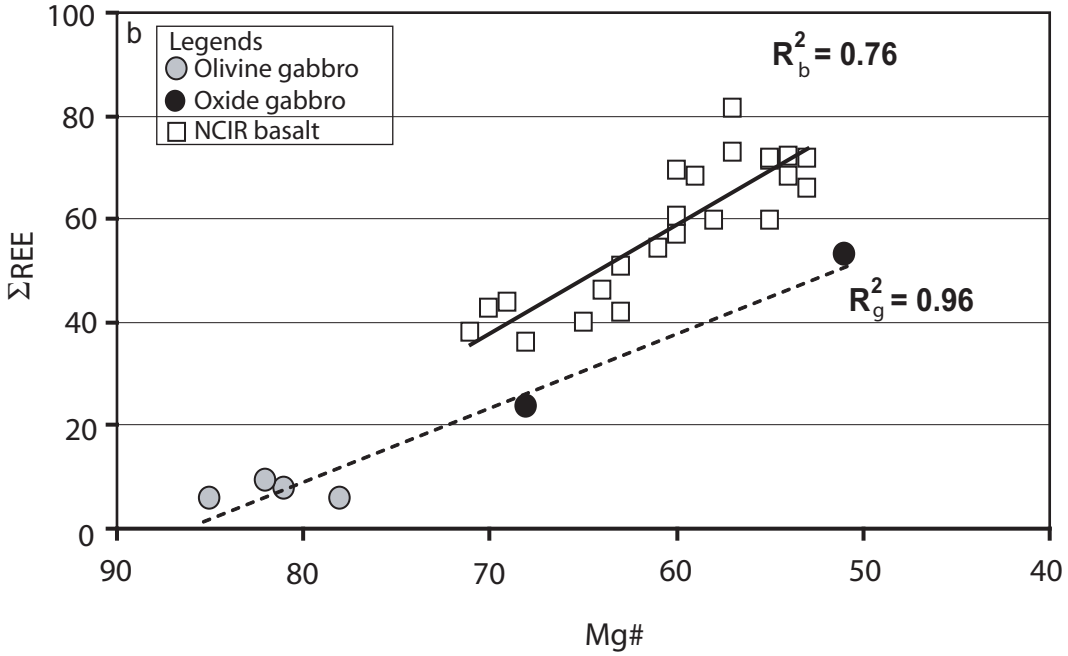
b
Legends
Olivine gabbro
Oxide gabbro
NCIR basalt
R^2_b = 0.76
R^2_g = 0.96
ΣREE
100
80
60
40
20
0
90
80
70
60
50
40
Mg#

Figure 9

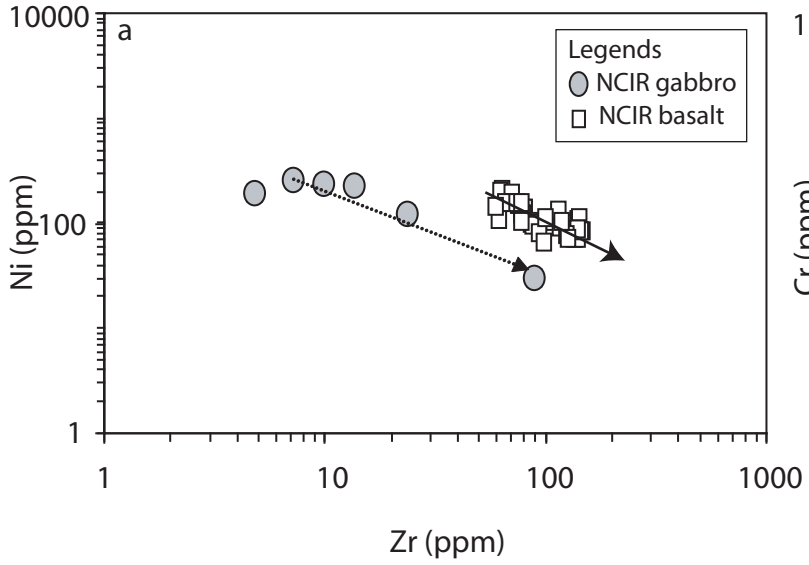
a
Legends
NCIR gabbro
NCIR basalt
Ni (ppm)
Zr (ppm)
10000
100
1
1
10
100
1000

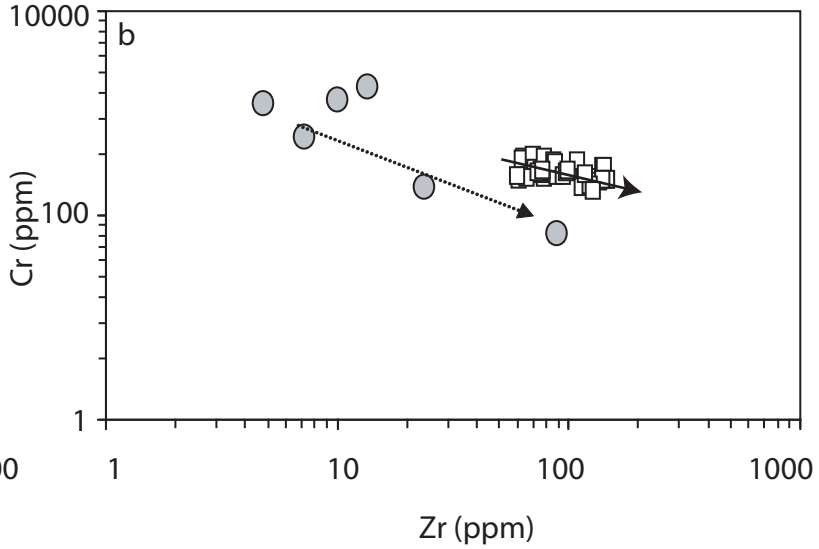
b
Cr (ppm)
Zr (ppm)
10000
100
1
1
10
100
1000

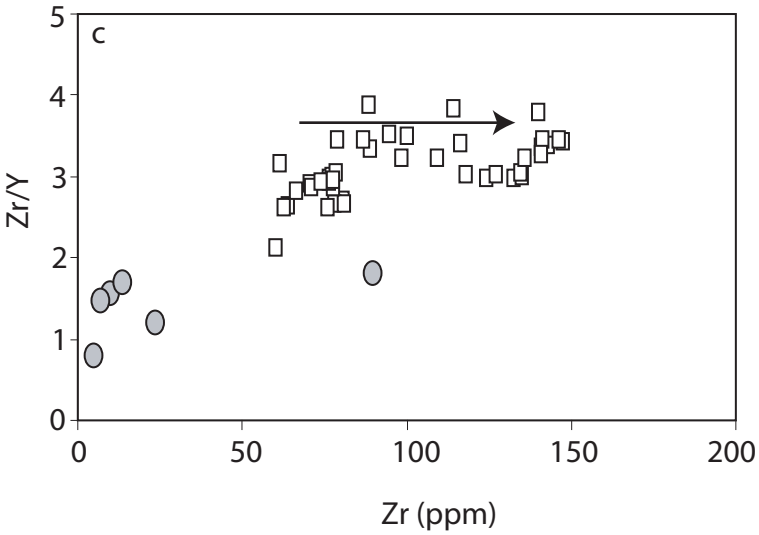
c
Zr/Y
Zr (ppm)
5
4
3
2
1
0
0
50
100
150
200

Figure 10

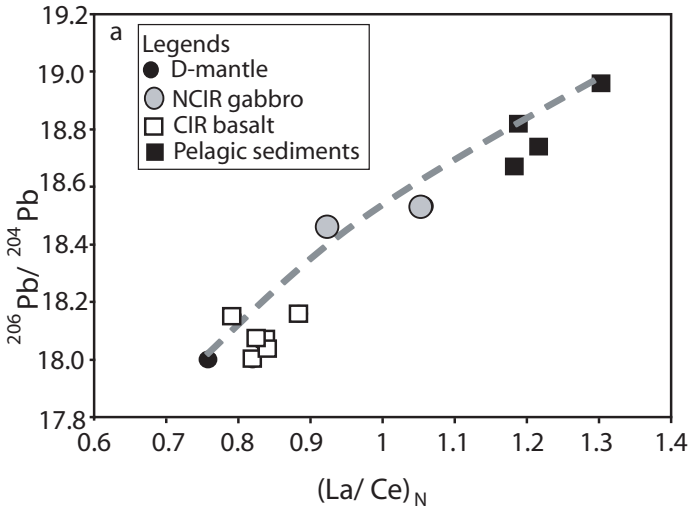
a
Legends
D-mantle
NCIR gabbro
CIR basalt
Pelagic sediments
19.2
19.0
18.8
18.6
18.4
18.2
18.0
17.8
$^{206}Pb/^{204}Pb$
0.6
0.7
0.8
0.9
1
1.1
1.2
1.3
1.4
$(La/Ce)_N$

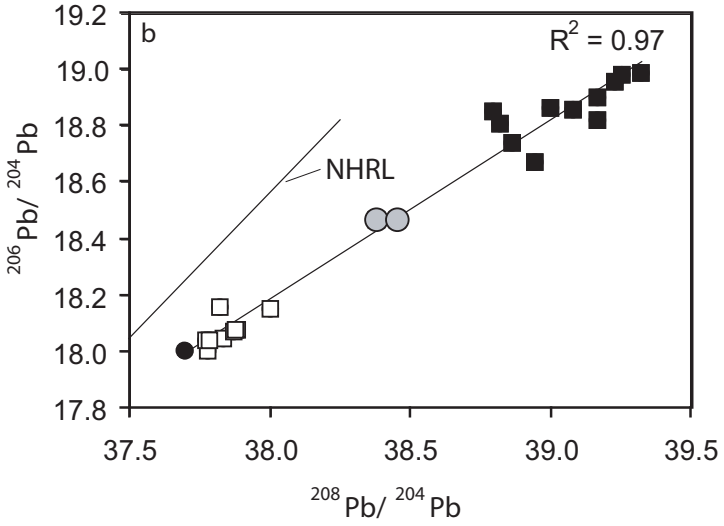
b
$R^2 = 0.97$
NHRL
19.2
19.0
18.8
18.6
18.4
18.2
18.0
17.8
$^{206}Pb/^{204}Pb$
37.5
38.0
38.5
39.0
39.5
$^{208}Pb/^{204}Pb$

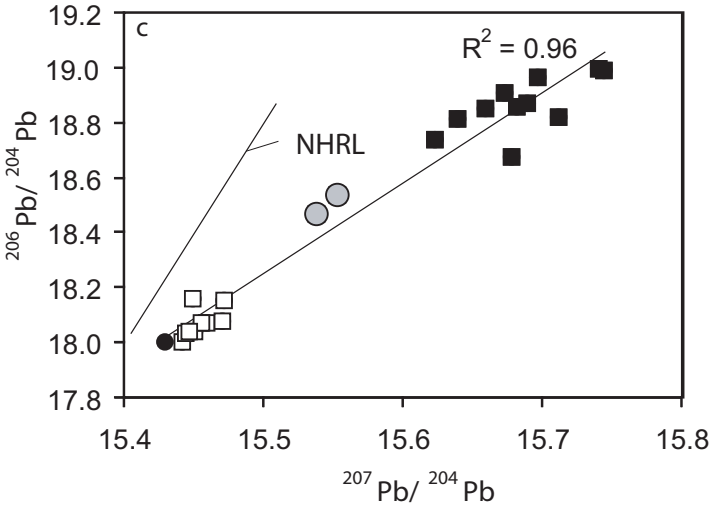
c
$R^2 = 0.96$
NHRL
19.2
19.0
18.8
18.6
18.4
18.2
18.0
17.8
$^{206}Pb/^{204}Pb$
15.4
15.5
15.6
15.7
15.8
$^{207}Pb/^{204}Pb$

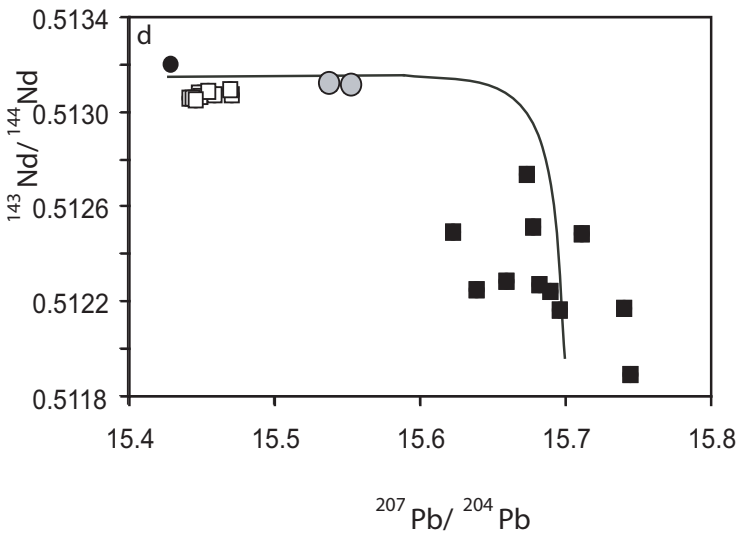
d
0.5134
0.5130
0.5126
0.5122
0.5118
$^{143}Nd/^{144}Nd$
15.4
15.5
15.6
15.7
15.8
$^{207}Pb/^{204}Pb$

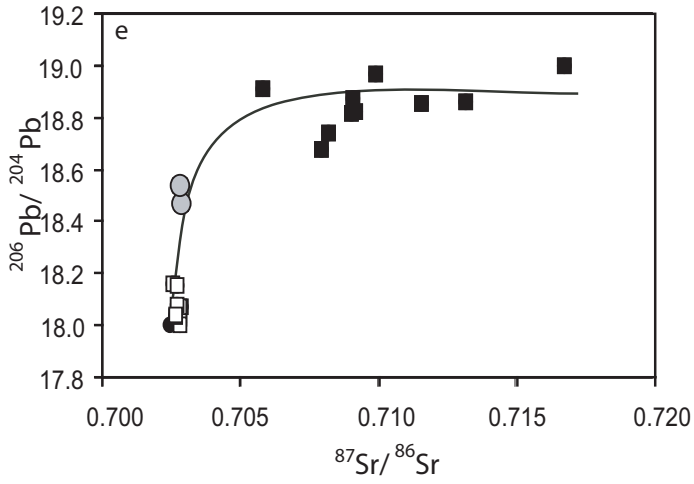
e
19.2
19.0
18.8
18.6
18.4
18.2
18.0
17.8
$^{206}Pb/^{204}Pb$
0.700
0.705
0.710
0.715
0.720
$^{87}Sr/^{86}Sr$

Figure 11